International Journal of Nanomedicine

Dovepress
open access to scientific and medical research

Open Access Full Text Article

ORIGINAL RESEARCH

Magnetic Graphene Oxide Nanocomposites Boosts Craniomaxillofacial Bone Regeneration by Modulating circAars/miR-128-3p/SMAD5 Signaling Axis

Yi He[1,2], Lejia Zhang[1,2], Siyuan Huang[1,2], Yuquan Tang[3], Yiming Li[1,2], Hongyu Li[1,2], Guanhui Chen[4], Xun Chen[1,2], Xiliu Zhang[1,2], Wei Zhao[1,2], Feilong Deng[1,2], Dongsheng Yu[1,2]

[1]Hospital of Stomatology, Guanghua School of Stomatology, Institute of Stomatological Research, Sun Yat-sen University, GuangZhou, 510080, People's Republic of China; [2]Guangdong Provincial Key Laboratory of Stomatology, Sun Yat-sen University, GuangZhou, 510080, People's Republic of China; [3]Zhujiang Hospital, Southern Medical University, Guangzhou, 510080, People's Republic of China; [4]Department of Stomatology, the Seventh Affiliated Hospital, Sun Yat-sen University, ShenZhen, 518107, People's Republic of China

Correspondence: Feilong Deng; Dongsheng Yu, Email dengfl@mail.sysu.edu.cn; yudsh@mail.sysu.edu.cn

Background: The ability of nanomaterials to induce osteogenic differentiation is limited, which seriously imped the repair of craniomaxillofacial bone defect. Magnetic graphene oxide (MGO) nanocomposites with the excellent physicochemical properties have great potential in bone tissue engineering. In this study, we aim to explore the craniomaxillofacial bone defect repairment effect of MGO nanocomposites and its underlying mechanism.

Methods: The biocompatibility of MGO nanocomposites was verified by CCK8, live/dead staining and cytoskeleton staining. The function of MGO nanocomposites induced osteogenic differentiation of BMSCs was investigated by ALP activity detection, mineralized nodules staining, detection of osteogenic genes and proteins, and immune-histochemical staining. BMSCs with or without MGO osteogenic differentiation induction were collected and subjected to high-throughput circular ribonucleic acids (circRNAs) sequencing, and then crucial circRNA circAars was screened and identified. Bioinformatics analysis, Dual-luciferase reporter assay, RNA binding protein immunoprecipitation (RIP), fluorescence in situ hybridization (FISH) and osteogenic-related examinations were used to further explore the ability of circAars to participate in MGO nanocomposites regulation of osteogenic differentiation of BMSCs and its potential mechanism. Furthermore, critical-sized calvarial defects were constructed and were performed to verify the osteogenic differentiation induction effects and its potential mechanism induced by MGO nanocomposites.

Results: We verify the good biocompatibility and osteogenic differentiation improvement effects of BMSCs mediated by MGO nanocomposites. Furthermore, a new circRNA-circAars, we find and identify, is obviously upregulated in BMSCs mediated by MGO nanocomposites. Silencing circAars could significantly decrease the osteogenic ability of MGO nanocomposites. The underlying mechanism involved circAars sponging miR-128-3p to regulate the expression of SMAD5, which played an important role in the repair craniomaxillofacial bone defects mediated by MGO nanocomposites.

Conclusion: We found that MGO nanocomposites regulated osteogenic differentiation of BMSCs via the circAars/miR-128-3p/SMAD5 pathway, which provided a feasible and effective strategy for the treatment of craniomaxillofacial bone defects.

Keywords: nanomaterials, MGO nanocomposites, craniomaxillofacial bone repair, circular RNAs, circAars

Introduction

Clinically speaking, critical-sized craniomaxillofacial bone defects are caused by traumatic tooth extractions, infection, oral cancer, and periodontal disease. Depending on the defect type, depth, and extension, the innate healing ability of the bone may be seriously influenced.[1] Established treatments based on the application of autografts have been used to accelerate regeneration and repair of the functional bone; however, the amount of unsatisfactory repairs is as high as

Received: 13 December 2023
Accepted: 20 March 2024
Published: 3 April 2024

Graphical Abstract

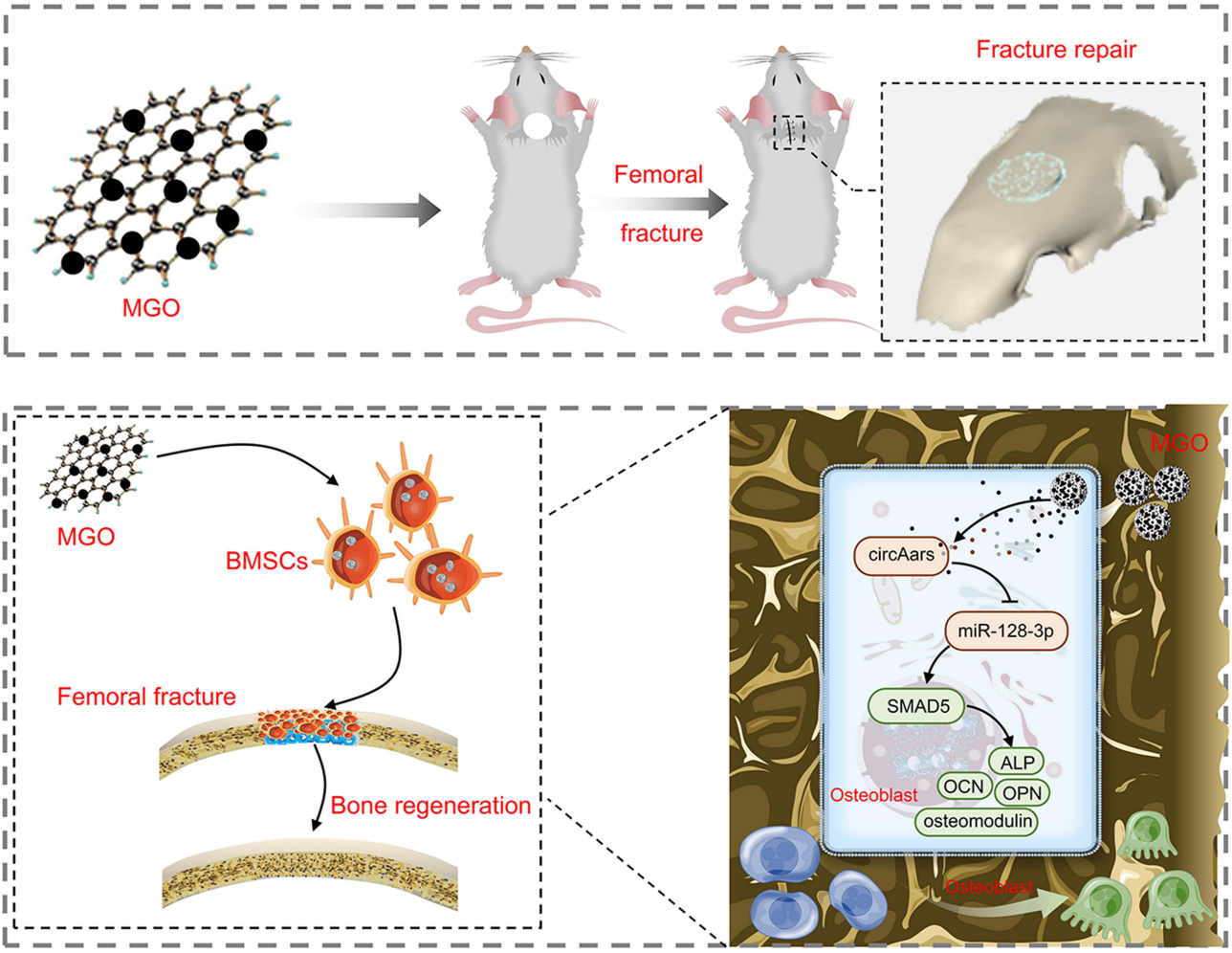

30%.[2] In current, bone tissue engineering (BTE) is a promising candidate to address this issue, including three essential elements of growth cytokines, biomaterials, and stromal cells.[3] The bone marrow mesenchymal stem cells (BMSCs) are "gold standard" cells are applied for bone regeneration.[4] However, some drawbacks exist that the self-renewal and proliferative capacities decreased with the increasing age, as well as the limited osteogenic capacity and uncertain efficacy of BMSCs. Therefore, it is urgent to search for a simple and effective method to improve osteogenic ability of BMSCs to repair the critical-sized craniomaxillofacial bone defects.

With the rapid development of nanotechnology, multiple nanomaterials have been used to BTE and adjusting cell proliferation, migration and osteogenic differentiation.[5,6] MGO as a novel kind of nanomaterials composed of magnetic nanoparticles and graphite oxide (GO), which hold the excellent physicochemical properties of biocompatibility, chemical stability, para-magnetism and ease of functionalization, which have a broadly potential in medical therapies.[7] MGO nanocomposites could be easily swallowed by dental pulp stem cells with no obvious effects on cell vitality and could deliver growth factors to improve cells osteogenic differentiation[8]. Recently, Zhang et al found that graphene oxide modified Fe_3O_4 could eliminate reactive oxygen species (ROS) in turn to improve the survival of mesenchymal stem cells compared with Fe_3O_4 alone.[9] In our previous study, we found that MGO nanocomposites could promote osteogenic differentiation of BMSCs in vitro, which was stronger than GO.[10] However, the ability of MGO nanocomposites to repair critical-sized craniomaxillofacial bone defects remains to be fully verified and the mechanism needs to be further explored.

Noncoding RNAs are a kind of RNA molecules that cannot be used as a translation template to complete protein synthesis in cells, which have a wide variety, rich content and mainly play a regulatory role. Through a wide range of complex mechanisms, they can participate in the regulation of any level from gene transcription to translation, and also have the function of regulating translation protein product.[11] Graphene materials and their derivatives can regulate the expression level of noncoding RNA, in turn to exert different biological functions.[12,13] As a kind of newly discovered noncoding RNAs, circRNAs are reverse splicing and not affected by RNA exonuclease and have a closed ring structure. Compared with long noncoding RNAs and miRNAs, their expression is more stable and difficult to degrade,[14] which are a rising star in maintaining stem cells pluripotency and regulating their multi-directional differentiation.[15–18] Recent studies have found that specific expression of circRNAs in inflammation,[16,19] stem cell osteogenic differentiation[20,21] and immunity.[22,23] Interestingly, our preliminary experiment found that circRNAs might participate in the process of MGO nanocomposites induced osteogenic differentiation of BMSCs through circRNAs high-throughput sequencing. Therefore, it is worthwhile to further uncover the role and mechanism of circRNAs in MGO nanocomposites induced osteogenic differentiation process. In terms of effects and mechanism, current researches showed that most exonic circRNAs are full of microRNA (miRNA) binding positions, which act as the function of miRNA "sponges" and then relieving the inhibition function of miRNA on its targets, which is known as competitive endogenous RNA (ceRNA) mechanism.[24] For example, Zhang et al found that circRNA-vgll3 could accelerate osteogenic capacity of adipose-derived mesenchymal stem cells (ADSCs) through regulating miR-326-5p/integrin α5 signaling axis.[25]

In this study, we aimed to explore the ability of MGO nanocomposites to repair critical-sized craniomaxillofacial bone defects and investigated the effects of circRNAs in regulating the osteogenic differentiation capacities induced by MGO nanocomposites as well as their underlying mechanisms. MGO nanocomposites showed good biocompatible with BMSCs and could promote the osteogenic ability of BMSCs to repair craniomaxillofacial bone defects. Mechanistically, a new circRNA circAars was found and circAars sponge miR-128-3p in turn to regulate the expression of SMAD5, which played a critical role in MGO-induced craniomaxillofacial bone regeneration process.

Materials and Methods

MGO Nanocomposites Preparation and Physicochemical Characterization

The MGO nanocomposites were synthesized via a chemical co-precipitation method.[7] In brief, 500 mg $FeCl_3 \cdot 6H_2O$ and 200 mg $FeCl_2 \cdot 4H_2O$ were stirred in pure water, and then to precipitate the iron oxides under N_2 atmosphere. The Fe_3O_4 nanoparticles received added gently to a 50 mL graphene oxide (GO) nanoparticles aqueous solution (1 mg/mL, XF-Nano, Nanjing, China) to produce the MGO nanocomposites, with magnetic stirring. Finally, MGO nanocomposites were received via a magnet and then dispersed in the distilled water. The size and morphology of MGO nanocomposites were examined through scanning electron microscope (SEM, Quanta 250 FEG, ThermoFisher Scientific, USA) and transmission electron microscopy (TEM, HT-7800, Hitachi, Japan). The chemical elements in MGO nanocomposites were analyzed using energy dispersive spectrometry (EDS, ThermoFisher Scientific, USA). The chemical functional groups of MGO nanocomposites were examined by a laser micro-Raman spectrometer (RAM II, Bruker, Germany) with 532 nm laser excitation and Fourier transformation infrared spectrometry (FTIR; IS50, ThermoFisher Scientific, USA). The surface zeta potential was determined using a nanoparticle analyzer (Zetasizer Nano ZSE, Malvern, Britain).

BMSCs Isolation and Identification

The cells in bone marrow of Sprague-Dawley rats (10–14 days old) were harvested with DMEM, which contain DMEM/F12 (Gibco, China), 1% penicillin/streptomycin (Gibco) and 10% fetal bovine serum (FBS, Gibco). BMSCs of passages 2–5 were applied in this study. The cell surface indications CD29, CD34, CD44, CD90 and CD45 (Biolegend, USA) were performed on flow cytometry (Beckman, Germany). Subsequently, osteogenic and adipogenic differentiation were used to determine multidirectional differentiation ability of cells.

Endocytosis and Prussian-Blue Staining

For endocytosis assay, MGO nanocomposites were labeled with Rhodamine B (Aladdin, USA) at room temperature and rinsing by PBS. BMSCs were treated with Rhodamine B labeled MGO nanocomposites for 24 hours. The cells underwent immobilization in 4% formaldehyde (Beyotime, Shanghai, China) and were then treated with actin-tracker green reagent (1:300, Beyotime) for 30 min and followed with DAPI (Beyotime) staining for 5 min in the dark. The cells treated were scanned by confocal laser scanning microscopy (CLSM, Zeiss, Germany).

For Prussian-blue staining, the BMSCs were cultured with MGO nanocomposites within 12 h and then fixed and washed. Subsequently, the cells were stained with Prussian-blue staining kit (Solarbio, Beijing, China) according to the manufacturer's protocol. Finally, an inverted microscopy (Olympus, Japan) was applied for observation.

Cell Viability and Proliferation

For Live/Dead assay, when BMSCs cultured with MGO nanocomposites with different densities within 48 h, calcein-AM in DMEM/F12 (1:1000, BestBio, Shanghai, China) was added to cells for 30 min, followed with propidium iodide (PI, BestBio) at the concentration of 1:2000 cultured on the samples for 5 min in the dark. An inverted microscope (Olympus) was applied to examine the fluorescence.

The proliferation of BMSCs treated with MGO nanocomposites was detected by CCK-8 (Dojindo, Japan). After incubation with different points, 10 μL of CCK-8 reagent and 90 μL of DMEM/F12 solution (Gibco) were added to each well. After incubating at 37°C for 2 h, cell viability was detected by measuring the optical density (OD) value at 450 nm by an automatic reader (BioTek Instruments, USA).

Osteoblastic Differentiation of BMSCs

For alkaline phosphatase (ALP) staining, the BMSCs with different treatments underwent immobilization and subsequently treated with a BCIP/NBT ALP staining kit (Beyotime) within 7 days of osteogenic induction, according to the manufacturer's instructions. An inverted microscope (Zeiss, Germany) was applied to examine the results. And then, ALP activity was detected by an ALP Assay kit (Jiangcheng Biotechnology, NanJing, China) according to the manufacturer's instructions. Briefly, BMSCs treated with osteogenic inducing medium (OIM) which contain DMEM, 50 μM of ascorbic acid, 100 nM of dexamethasone and 10 mM of β-glycerophosphate (Sigma, USA). After 7 days, the cells were harvested in RIPA solution (CWBIO, Beijing, China) and then were applied to detect ALP activity according to the operating manual.

For alizarin red staining (ARS), after osteogenic inducing for 14 days, the samples with different treatments underwent immobilization. Subsequently, samples were treated with alizarin red (Cyagen) within 60 min at room temperature, and a microscopy (Zeiss, German) was used to observe of the calcified nodules. The stained mineral nodules were subsequently dissolved using 10% cetylpyridinium chloride solution (Sigma-Aldrich) for 1 h, and the OD value of solution was detected at 562 nm by using an automatic reader.

For cellular immunofluorescence staining, BMSCs were cultured on confocal dish and fixed by incubating with paraformaldehyde for 30 min. Fixed cells were then rinsed with phosphate balanced solution (PBS) and permeabilized using 0.1% Triton X-100 in PBS for 10 min. Cells were then blocked by incubating with 10% goat serum (Scientific research, USA) within 30 min and treated with primary antibody, which including ALP (1:200, Affinity, USA), Runx2 (1:200, Affinity) and SMAD5 (1:200, Affinity). Cells were then rinsed with PBS and treated with the suitable fluorescein-conjugated secondary antibody. The images were observed by CLSM (Olympus, Japan).

CircRNA-Sequencing

The sequencing was completed by Beijing Capital Biotechnology Co., Ltd (Beijing, China). Briefly, RNA was received from three pairs of BMSCs which were treated with OIM containing 0.1 μg/mL MGO nanocomposites or not after 7 days. In brief, the NEBNext Ultra RNA Library Prep Kit for Illumina (NEB, USA) was applied to form the libraries for sequencing following manufacturer's instructions. The RNA was fragmented into pieces of ~200 base pair in length in NEBNext First Strand Synthesis Reaction reagent (5X). The end of the cDNA pieces was undergone an end repair

procedure, followed by ligation of the adapters. The products received were purified and amplified through polymerase chain reaction to amplify the library DNA. The libraries we constructed were qualified by Agilent 2100 and quantified by KAPA Library Quantification kit (KAPA Biosystems, South Africa). Finally, the libraries were subjected to paired-end sequencing with pair end 150-base pair reading length on an Illumina NovaSeq sequencer (Illumina, San Diego, CA, USA). CircRNAs with FC $\geq$ 2, and p values <0.05 were identified as obviously differential. Additionally, all PCR amplification products were examined for identification of circAars using Sanger sequencing, RT-PCR and qPCR.

Cells Transfection

RNA transient transfection with 2.5 μg circAars overexpression plasmid or 50 nM si-circAars, 50 nM miR-128-3p mimic, 50 nM miR-128-3p inhibitor or 50 nM si-SMAD5 (RiboBio Co., Ltd. Guangzhou, China) by Lipofectamine 3000 (Invitrogen, Carlsbad, CA, USA) at the basis of the manufacturer's protocol and then were used for further experiments. The sequence of transfection reagents was shown in Table 1.

RNA Binding Protein Immunoprecipitation (RIP)

RIP experiment was examined with a Magna RIP RNA binding protein immunoprecipitation kit (Millipore, Billerica, USA) through the protocols. BMSCs were received and underwent harvested in RIP lysis solution, and then the productions we extracted were separately treated with RIP immunoprecipitation solution containing magnetic beads conjugated with negative control normal mouse immunoglobulin G (IgG, Millipore) and Argonaute2 (AGO2) antibody (Abcam, Britain). Subsequently, the samples were treated with Proteinase K, following with the RNA immunoprecipitation fraction was purified. At final, the RNAs we received were examined using qPCR to detect the expression level of circAars and miR-128-3p.

Table 1 Constructed Sequences Used in This Study

Name	Sequence (5′-3′)
si-circAars-1	CCAAACCATCCCAGGGAAT
si-circAars-2	CCATCCCAGGGAATCTGAT
si-circAars-3	AAACCATCCCAGGGAATCT
miR-128-3p mimic	UCACAGUGAACCGGUCUCUUU
	AAAGAGACCGGUUCACUGUGA
miR-128-3p inhibitor	AAAGAGACCGGUUCACUGUGA
si-SMAD5-1	GGAAAGGTGTCCATCTATA
si-SMAD5-2	GCTAAAGCCTTTGGATATT
si-SMAD5-3	GGTGTTCGATTGTGTACTA
circAars	GGAATCTGATGGTGTTCTGAAACCTCTCCC
	CAAGAAAAGCATTGACACAGGGATGGGCCT
	GGAGAGATTGGTGTCTGTGCTGCAGAACAA
	GATGTCCAACTATGACACTGACCTTTTCGTT
	CCTTACTTCGAAGCCATTCAGAAGGGTACAG
	GCGCCCGGCCGTATACTGGGAAGGTTGGTGC
	TGAGGACACTGATGGAATTGACATGGCCTACA
	GGGTTCTGGCTGACCACGCCCGGACCATCACT
	GTGGCGCTGGCTGATGGCGGGCGACCTGACAA
	CACAGGTCGGGGGTATGTGCTGAGACGGATCCT
	TCGCCGAGCTGTTCGCTATTCCCACGAGAAACT
	GAACGCCAGCAGGGGTTTCTTCGCCACATTAGTT
	GATGTTGTCGTTCAATCCCTGGGAGACGCCTTTC
	CTGAGCTGAAGAAGGACCCAGATATGGTGAAGGA
	CATCATTAATGAAGAAGAGGTACAGTTTCTCAAGA
	CTCTCAGCAGAGGGCGGCGCATCCTGGACCGGAAA
	ATTCAGAGCTTAGGAGACTGCCAAACCATCCCAG.

Luciferase Reporter Experiment

Luciferase reporter assays were taken for the examination of direct target sites between circAars and miR-128-3p or between miR-128-3p and SMAD5. psi-CHECK2 vectors (Promega, Madison, USA) with firefly luciferase and Renilla luciferase gene were used in the present assay. Sequence of circAars and SMAD5 were all cloned into psiCHECK-2 vectors, and miR-128-3p inhibitor and mimic were used. Mutations of circAars and SMAD5 were constructed in the binding position and were then co-transfected into 293T cells at the same time. Within 48 h of co-transfection, the luciferase activities were detected through the dual-luciferase reporter experiment (Promega, USA).

Fluorescence in situ Hybridization (FISH)

FISH assay was performed to evaluate the expression of circAars with a FAM-labeled probe (5'-CATCAGATTCCCTGGGATGGTTTGGC-3') and the expression of miR-128-3p with a Cy3-labeled probe (5'-AAAGAGACCGGTTCACTGTGA-3'), respectively. In brief, BMSCs and skull paraffin sample underwent immobilization with 4% paraformaldehyde and then hybridized at 37°C overnight with specific probes. Subsequently, the samples were rinsed with 2x SSC/formamide, treated with anti-DIG-HRP (PerkinElmer, Boston, MA, USA), then treated with TSA fluorescent reagent (PerkinElmer), and then stained with 4,6-diamidino-2-phenylindole (DAPI). At final, the results were observed with CLSM (Olympus).

qPCR

The RNA was isolated by RNAzol reagent (Molecular Research Center, USA), and cDNA was synthesized using the cDNA synthesis kit (TaKaRa, Tokyo, Japan) according to the protocols. The expression levels of circRNAs and mRNAs were normalized to GAPDH, and microRNAs (miRNAs) expression was normalized to U6. The all sequences applied are showed in Table 2. cDNA amplification procedure was carried out with the SYBR Green Reagent kit (Takara) following the operating manual. Data were performed by calculating the $2^{-\Delta\Delta Ct}$ relative fold change.

Table 2 Primers Used for Quantitative RT-PCR Assays

Gene	Sequence (5′-3′)
GAPDH-Forward	AACCTGCCAAGTATGATGA
GAPDH-Reverse	GGAGTTGCTGTTGAAGTC
β-catenin-Forward	GGACAAGCCACAGGATTAC
β-catenin-Reverse	CAGTCTCATTCCAAGCCATT
Runx2-Forward	TACTTCGTCAGCATCCTA
Runx2-Reverse	CGTCAACACCATCATTCT
BMP-2-Forward	GAATCAGAACACAAGTCAGT
BMP-2-Reverse	GACCTGCTAATCCTCACA
OCN-Forward	CTCACTCTGCTGGCCCTGAC
OCN-Reverse	CACCTTACTGCCCTCCTGCTTG
Osteomodulin-Forward	AGGTTGTGCTAAGGAATG
Osteomodulin-Reverse	GTTGAGTTGCTGAATGTG
OPN-Forward	AATGCTGTGTCCTCTGAA
OPN-Reverse	TCGTCATCATCATCGTCAT
SMAD5-Forward	CTGCTGTCCAACGTTAATCG
SMAD5-Reverse	GAACAAAGATGCTGCTGTCA
circTll1-Forward	AGGCCTTTGAGATTGTCTTGA
circTll1-Reverse	TGAGAACTCCAGCCACTTTG
circAars-Forward	GGGGTTTCTTCGCCACATTA
circAars-Reverse	ATCAGATTCCCTGGGATGGT
circDysf-Forward	GAGAACTTCCTGTGTGACCC

(*Continued*)

Table 2 (Continued).

Gene	Sequence (5′-3′)
circDysf-Reverse	CTGTGTCCTCCGTCTGGA
circCnot4-Forward	AACCACTTTCCCAGGAAGAA
circCnot4-Reverse	CTCTGAAGACTTCTGGGTCTG
circStk38l-Forward	AGTGGTTGGTCGGACAGTTA
circStk38l-Reverse	CTGCCACAGTGAGTTTAGGC
circRfwd2-Forward	TAACTCTGTAAGACCGTTGGC
circRfwd2-Reverse	CAAATTGAGGCACCGTGCTA
circPlce1-Forward	GCTTGGAGTTACGTCGATCA
circPlce1-Reverse	GTGTTTTCTGTTCCCAGACAC
circUck2-Forward	GTCTCGCAGAGTCTTCCGTG
circUck2-Reverse	CCGGGTGATCGAAGTTGAAT
circBend6-Forward	AGGAAACCCCCTTAGTGGAA
circBend6-Reverse	TGCTCCTTGCAGCATGAC
circTbc1d1-Forward	AAGAACACAAACAGGGACTT
circTbc1d1-Reverse	CTGCTCGTTTCTTGGTCTCA
U6-Forward	CTCGCTTCGGCAGCACA
U6-Reverse	AACGCTTCACGAATTTGCGT
U6-RT	AACGCTTCACGAATTTGCGT
miRNA-Reverse	CTCAACTGGTGTCGTGGA
miR-216b-5p-Forward	ACACTCCAGCTGGGAAATCTCTGCAGGCAAATGTCACATTT
miR-216b-5p-RT	CTCAACTGGTGTCGTGGAGTCGGCAATTCAGTTGA
miR-1956-5p-Forward	ACACTCCAGCTGGGAGTCCAGGGCTGAGTCAGC
miR-1956-5p-RT	CTCAACTGGTGTCGTGGAGTCGGCAATTCAGTTGAGTCCGCTGA
miR-34a-5p-Forward	ACACTCCAGCTGGGTGGCAGTGTCTTAGCTGGT
miR-34a-5p-RT	CTCAACTGGTGTCGTGGAGTCGGCAATTCAGTTGAGTCACATTT
miR-17-1-3p-Forward	ACACTCCAGCTGGGACTGCAGTGAAGGCACTT
miR-17-1-3p-RT	CTCAACTGGTGTCGTGGAGTCGGCAATTCAGTTGAGCCACAAGTG
miR-128-3p-Forward	ACACTCCAGCTGGGTCACAGTGAACCGGTCTC
miR-128-3p-RT	CTCAACTGGTGTCGTGGAGTCGGCAATTCAGTTGAGAAAGAGAC
miR-3065-3p-Forward	ACACTCCAGCTGGGTCAGCACCAGGATATTGTTG
miR-3065-3p-RT	CTCAACTGGTGTCGTGGAGTCGGCAATTCAGTTGAGTCCCCAACAA
miR-340-3p-Forward	ACACTCCAGCTGGGTCCGTCTCAGTTACTTTAT
miR-340-3p-RT	CTCAACTGGTGTCGTGGAGTCGGCAATTCAGTTGAGGGCTATAAAGCTCAAC

Western Blot Analysis

The proteins were extracted with RIPA buffer through a lysis solution (CWBIO) containing 1% proteinase inhibitor (CWBIO) and quantified using a BCA protein assay kit (CWBIO). Proteins received in equal quantities were isolated by 10% SDS-PAGE gradient gels (CWBIO) and electro-transferred to a nitrocellulose membrane. After blocking nonspecific binding using 5% non-fat milk in distilled water for 1 h, membranes were hybridized at 4 °C overnight with special diluted primary antibodies. The primary antibodies used included β-catenin (1:2000, Cell Signaling, USA), runt-related transcription factor 2 (Runx2, 1:1000, Cell Signaling), bone morphogenetic protein (BMP2, 1:500, Abcam, USA), SMAD5 (1:500, Cell Signaling) and GAPDH (1:2000, Cell Signaling). After rinsing with TBST (CWBIO), membranes were treated with the suitable horseradish peroxidase (HRP)-conjugated secondary antibody (1:3000, Cell Signaling) at room temperature for 1 h. The expression of protein in the groups was quantified by Image-J, and GAPDH was used as an internal loading control.

In vivo Bone Formation Assay

Animals applied in this study were followed the Guideline for ethical review of animal welfare of laboratory animals published by the China National Standardization Management Committee (publication No. GB/T 35892–2018). These

experiments were approved by the Biological and Medical Ethics Committee, Sun Yat-sen University (SYSU-IACUC-2021-000271). BMSCs treated with MGO nanocomposites within 7 days before the assay in vivo. The cells after treatment with a concentration of 2*10^6 were seeded in β-tricalcium phosphate scaffold overnight (β-TCP, Melone, China) with a size of 5 mm × 5 mm× 1 mm, a trabecular diameter of 400 μm, and a pore size of 500 μm. About 6-weeks-old male Sprague-Dawley rats (200–250g) were received from Vital River Laboratory Animal Technology Co. (Beijing, China) and randomly isolated into three groups, including growth medium group (GM), OIM group and MGO/OIM group. Rats were provided with standard food and distilled water and were kept in a room under conditions of maintained humidity (68–72%) and temperature (about 25 °C). After separating the pericranium, critical-sized calvarial defects (Φ = 5 mm) were constructed through a dental drill under general anesthesia using Zoletil-50 (40 mg/kg, Virbac S.A. France). The BMSCs-loaded scaffolds we prepared were then put into the defects. Periosteum and skin were closely sutured layer by layer, and penicillin sodium was injected for 3 consecutive days after operation. The physical condition of rats was observed regularly every 7 days after operation. Eight weeks after operation, the rats were sacrificed with cervical dislocation after excessive anesthesia by Zoletil-50. The skulls were received and fixed in 4% paraformaldehyde. Images scanned at a valid pixel size of 10 μm at 70 kV, 114 μA, and with a 1500-ms exposure time using a high-resolution Inveon Micro-CT (Siemens, Munich, Germany). Three-dimensional reconstruction and bone parameter analysis were constructed with a professional three-dimensional analysis software (Siemens).

For Hematoxylin and eosin staining, Masson's trichrome staining, and immune-histochemical staining analyses. In brief, the samples received were decalcified with 10% ethylene diamine tetraacetic acid within 2 months, and then dehydrated and treated with paraffin. The pieces were isolated at 5 μm thickness and treated with hematoxylin and eosin (H&E) and Masson's trichrome. The immunohistochemistry staining was performed using β-catenin (1:200, Affinity Bioscience), Runx2 (1:200, Affinity), BMP2 (1:200, Affinity) and SMAD5 antibodies (1:200, Affinity). All outcomes were examined through a ScanScope XT tissue slide scanner (Aperio, Leica Biosystems, Buffalo Grove, USA).

Statistical Analysis

Statistical significances were calculating with one-way analysis of variance accompanied by the LSD test and a two-tailed Student's *t*-tests with SPSS software from IBM Corp. The results were showed with average ± standard deviations (SD) and a $p < 0.05$ between groups were set to be statistically significant.

Results

Characterizations of BMSCs and MGO Nanocomposites

BMSCs exhibited a long spindle shape, typical fibroblast morphology (Figure 1A) and had the potential for multi-directional differentiation into osteoblasts and adipocytes (Figure 1B). Cell surface antigen markers CD34 (1.57%) and CD45 (2.63%) showed negative, while CD44 (99.89%), and CD90 (99.93%) showed strong positivity (Figure 1C). The above results showed that BMSCs were successfully extracted.

The SEM results indicated that MGO nanocomposites were distributed in a granular manner with relatively uniform particle distribution (Figure 1D). The energy spectrum analysis results indicated that Fe, C, and O elements are accounting for 38.94%, 11.82%, and 49.24% in MGO nanocomposites, respectively (Figure 1E). Typical TEM images showed that a thin layer GO was located at the bottoms of the Fe_3O_4 with an average diameter of about 15 nm (Figure 1F and G). FTIR analysis revealed the characteristic C=C and Fe-O bonds in MGO nanocomposites (Figure 1H). Raman spectrum results showed that there were obvious D peak and G peak structures in MGO nanocomposites, which are typical characteristics of GO (Figure 1I). Zeta potential analysis showed that the potential of MGO nanocomposites in DMEM was −11.61 ± 0.86 mV (Figure 1J). Prussian-blue assay showed that MGO was mainly existed in the cytoplasm of BMSCs (Figure 1K). Meanwhile, endocytosis experiment showed that MGO nanocomposites could be internalized by BMSCs and were mostly located in the cytoplasm (Figure 1L).

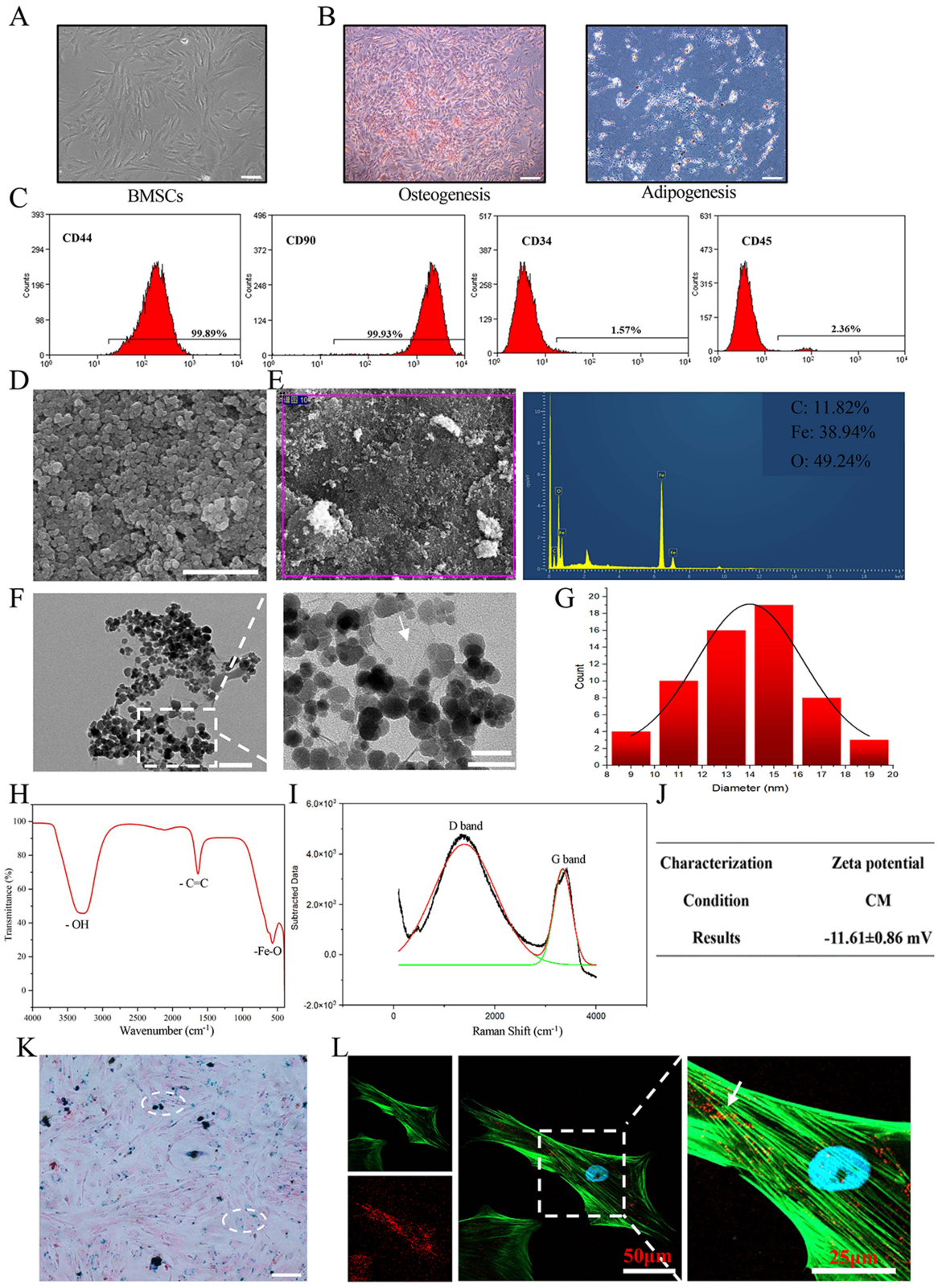

Figure 1 Characterization of BMSCs and MGO nanocomposites. (**A**) Typical morphologic features of BMSCs. Scale bar = 100 μm. (**B**) Multi-potential differentiation capacities were examined. Scale bar = 200 μm.(**C**) Immuno-phenotypic characteristics examination through Flow cytometry. (**D**) Representative images of MGO nanocomposites by SEM. Scale bar = 1 μm. (**E**) The chemical elements were analyzed by EDS. (**F**) Representative images of MGO nanocomposites by TEM, Scale bar = 100 nm. (**G**) Particle size analysis. (**H**) The chemical functional groups were examined through FTIR. (**I**) Structure of MGO nanocomposites were examined using laser micro-Raman Spectrometer. (**J**) Zeta potential analysis. (**K**) Typical Prussian-blue staining. Scale bar = 100 μm. (**L**) Detection of endocytotic MGO nano-composites ability of BMSCs. The MGO showing with red; Cytoskeleton showing with green and nuclei stained with blue. Scale bar = 50 μm.

https://doi.org/10.2147/IJN.S454718 DovePress

In vitro Cytocompatibility and Osteogenic Capacity Potential

The cytocompatibility of MGO nanocomposites was explored. The live/dead assay demonstrated that the proportion of live cells and dead cells in MGO nanocomposites groups showed no obvious significance compared with the control group (Figure 2A and B). The distribution of adhesion proportion and morphology of BMSCs also demonstrated no obvious difference after MGO nanocomposites treatments (Figure 2C). Cell proliferation ability of BMSCs was examined through CCK-8 assay after culturing for 1, 3, 5, and 7 d. The results showed that after treatment with MGO nanocomposites, BMSCs showed no significant difference in the number of cell proliferation compared to the control group at the first 5 days; And at 7th day, 0.1 μg/mL MGO nanocomposites significantly promoted the proliferation of BMSCs (Figure 2D). The above results showed that MGO nanocomposites were good biocompatible with BMSCs.

After osteogenic inducing, ALP staining (Figure 2E) and ALP activity (Figure 2F) outcomes suggested that MGO nanocomposites could promote osteogenic capacity of BMSCs and this effect was more apparent in 0.1 μg/mL group, which showed the same trend according to the mineralized nodules staining (Figure 2G and H). Furthermore, the osteogenic genes level of β-catenin, OCN, Runx2, OPN, BMP2 and osteomodulin were significantly up-regulated in the MGO group (Figure 1I). Meanwhile, the expression proteins were examined (Figure 2J and K), which showed that MGO apparently accelerated the expression of β-catenin, Runx2 and BMP2 level. Immunofluorescence results also demonstrated that the expression of ALP (Figure 2L and M) and Runx2 (Figure 2N and O) most obviously accelerated in MGO group.

Collectively, these results highlighted that MGO nanocomposites had the ability to induce osteogenic differentiation in vitro, and this osteogenic induction effect might be more apparent in the 0.1 μg/mL group.

Dysregulated circRNAs and Increased circAars in MGO Nanocomposites Induced Osteogenic Capacity

To investigate the role of circRNAs in the osteogenic differentiation ability of MGO nanocomposites, two groups of BMSCs, with three biological replicates in each subset, were received for transcriptome sequencing through RNA-sequencing. The two subsets included: OIM group (culture with osteogenic induction medium) and MGO/OIM group (culture with 0.1 μg/mL MGO nanocomposites containing osteogenic induction medium) for 7 days. Differential gene expression profiling was shown in Figure 3A. Volcano map showed that 46 differential express of circRNAs with fold change (FC) ≥2 and p <0.05 were found, among which 23 downregulated and 20 were upregulated (Figure 3B). To screen the critically differential circRNAs, the level of five representational changed circRNAs were selected to validate their expression. Among them, the level of circAars, we termed was significantly and consistently upregulated in MGO-induced BMSCs (Figure 3C and D), so we focused on the circAars in the subsequently experiment, and then the characteristics of circAars was examined. Additionally, through using specially designed convergent; divergent primers and RNase R digestion, the results showed that even after using RNase R treatment, circAars could be only found in cDNA, meanwhile no outcomes were found in the genomic DNA in BMSCs, which suggested that circAars could resist RNase R treatment and it was not the outcome of genomic rearrangements and trans-splicing (Figure 3E and F). CircAars was spliced from the Aars gene on chromosome 19: 43205059-43206857. Moreover, we identified that the head-to-tail splicing of circAars and genomic sizes and sequence using Sanger sequencing (Figure 3G). The outcomes through FISH assay demonstrated that the expression of circAars was mainly existed in cytoplasm of BMSCs (Figure 3H). These above findings suggested that circAars might act a critical role in MGO nanocomposites induced osteogenic differentiation improvement process.

circAars Inhibition Decreased the Osteogenic Capacity of MGO Nanocomposites

For evaluating the function of circAars in osteogenic differentiation induced by MGO nanocomposites, after circAars silencing, we cultured BMSCs under OIM or MGO/OIM condition. The expression of circAars could statistically silenced by using si-circAars-1 and si-circAars-3 in BMSCs (Figure 4A). The ALP staining (Figure 4B) and ALP activity (Figure 4D) showed that circAars silencing caused a significant osteogenic differentiation inhibition of BMSCs both in OIM and MGO condition. Meanwhile, we found that less mineralized nodules in the BMSCs when the circAars

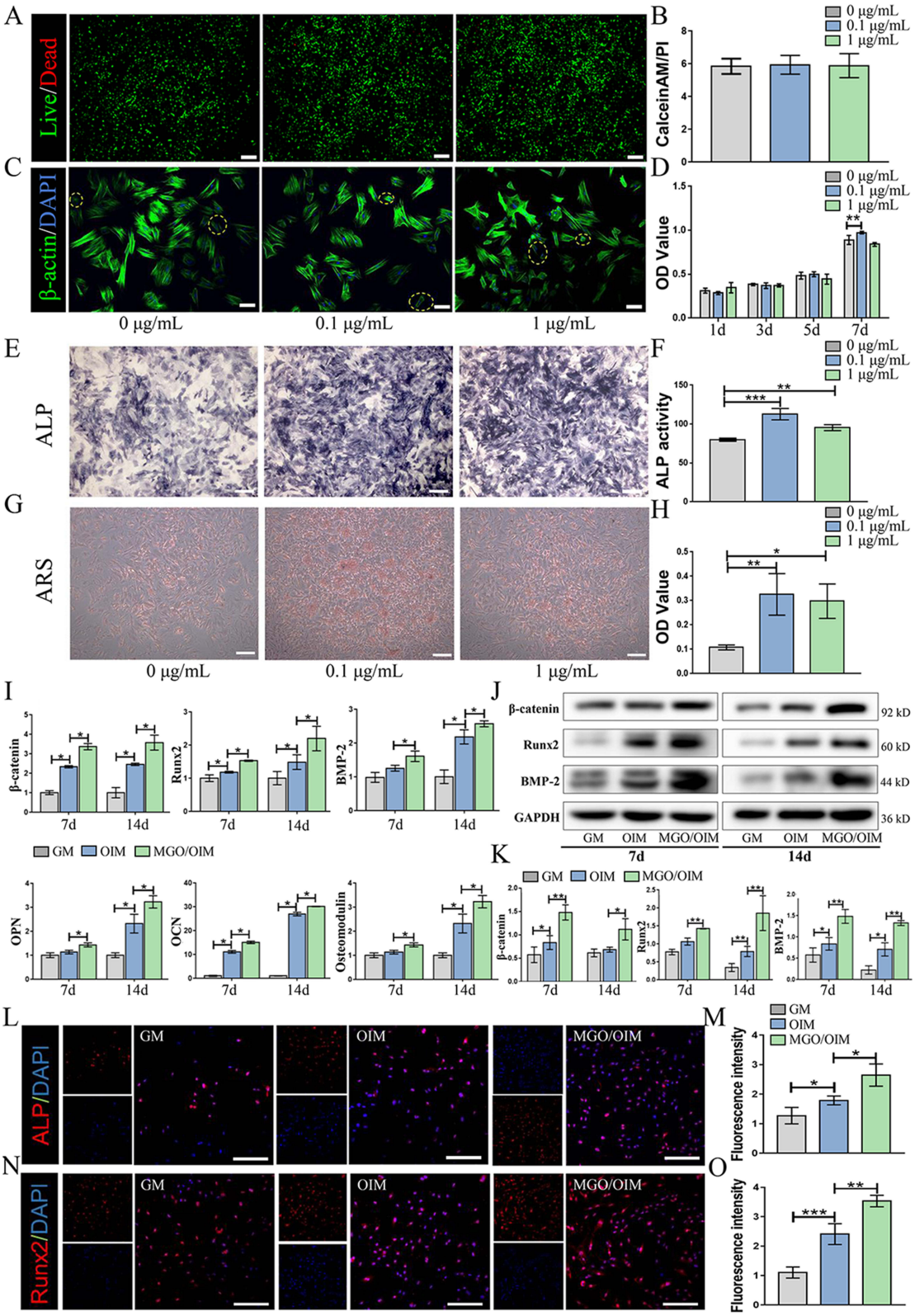

Figure 2 In vitro cytocompatibility and osteogenic capacity potential. (**A** and **B**) Live/dead staining assay of BMSCs culture with MGO nanocomposites. Scale bar = 200 μm. Live cells stained green and dead cells stained red. (**C**) Cytoskeleton of BMSCs after culture with MGO nanocomposites. Cytoskeleton showing with green and nuclei stained blue. The yellow circle indicating the shrinking cells. Scale bar = 100 μm. (**D**) CCK-8 detected the proliferation effect of BMSCs cultured with MGO nanocomposites. (**E** and **F**) The ALP staining and ALP activity examination. Scale bar = 200 μm. (**G** and **H**) ARS staining and semi-quantitative analysis. Scale bar = 200 μm. (**I**) The osteogenic-related mRNA expression was examined by qPCR. (**J** and **K**) The osteogenic-related proteins expression was determined by western-blot. (**L** and **M**) Cellular immunofluorescence assay showing the cellular expression of ALP and (**N** and **O**) Runx2. Scale bar = 100 μm. The results are presented as mean ± SD (*P<0.05, **P<0.01, ***P<0.001).

https://doi.org/10.2147/IJN.S454718 DovePress

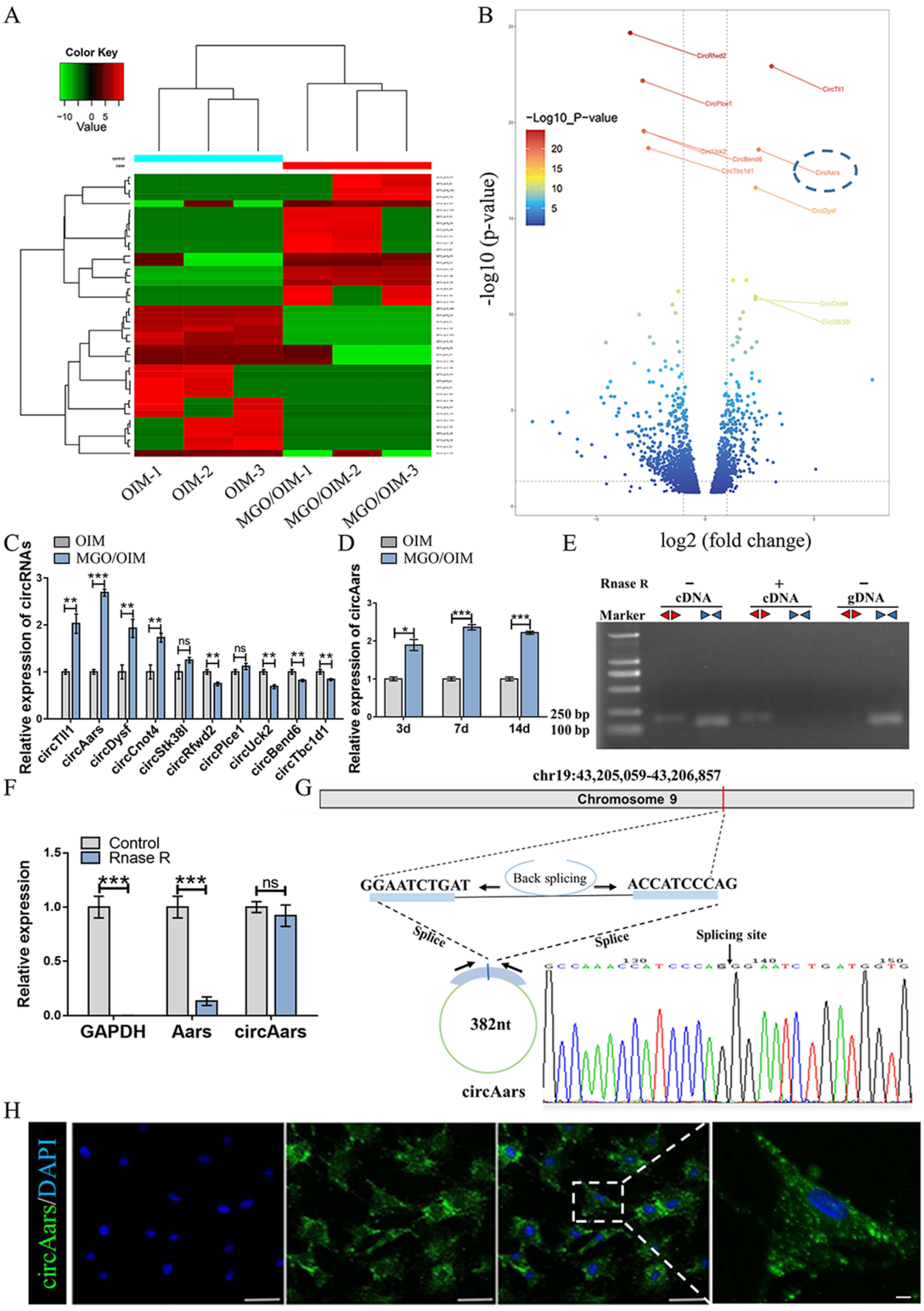

Figure 3 Dysregulated circRNAs and increased circAars in MGO nanocomposites induced osteogenic capacity. (**A**) Heatmap analyses of RNA-seq showing differentially expressed circRNAs with fold changes >2.0. Each row indicates the expression of a circRNA and each column indicates a cell specimen. The green to red represents intensity which increased from low to high. (**B**) Volcano plot visualizes the representative differential circRNAs. The horizontal purple line indicated a p value of 0.05, and the vertical purple lines indicated 2-fold down and up. (**C**) qPCR analysis detected the expression level of five representative differential circRNAs in BMSCs treated with MGO. (**D**) qPCR analysis of circAars expression in BMSCs treated with MGO at different time points. (**E**) The detection of circAars in the absence or presence of RNase R in complementary deoxyribonucleic acid (cDNA) and genomic deoxyribonucleic acid (gDNA) from BMSCs using RT-PCR. (**F**) qPCR analysis of circAars expression in BMSCs treated with RNase R. (**G**) Schematic illustration demonstrating the formation of circAars and RT-PCR outcomes were determined through Sanger sequencing. (**H**) The expression of circAars in BMSCs was detected by FISH. Scale bar = 50 μm. The results are presented as mean ± SD (*P<0.05, **P<0.01, ***P<0.001).

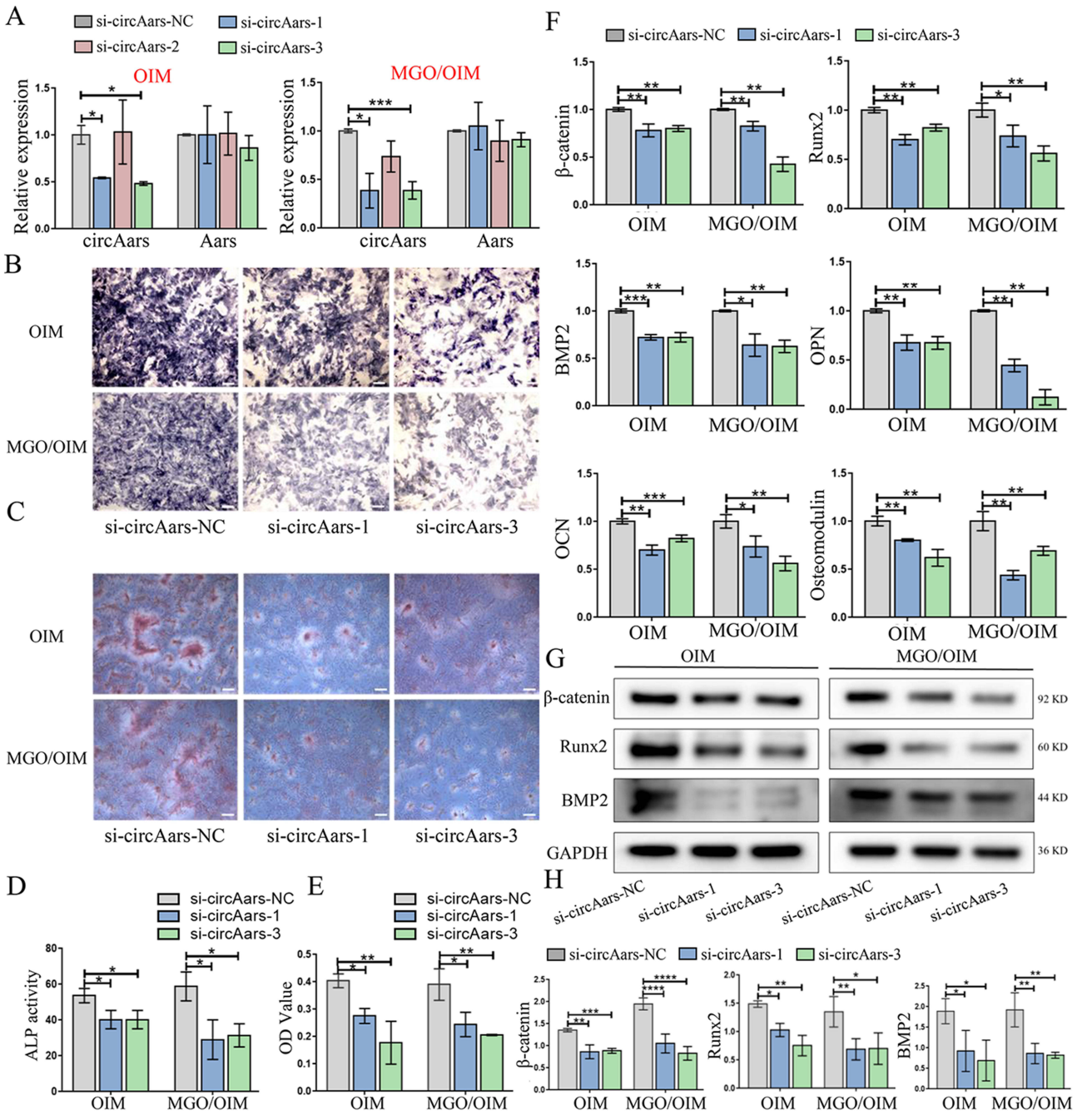

Figure 4 CircAars inhibition decreased the osteogenic capacity of MGO nanocomposites in BMSCs culturing in osteogenic medium with or without the addition of MGO nanocomposites. (**A**) qPCR determined the silencing efficiency of circAars. (**B** and **D**) The ALP staining and quantitative analysis was determined in BMSCs transfected with si-circAars-NC and si-circAars in cells culturing in osteogenic medium with or without the addition of MGO nanocomposites. Scale bar = 200 μm. (**C** and **E**) ARS staining and semi-quantitative analysis. Scale bar = 200 μm. (**F**) Osteogenic-related mRNA expression level was detected. (**G** and **H**) Osteogenic-related proteins expression level was determined. The results are presented as mean ± SD (*P<0.05, **P<0.01, ***P<0.001).

inhibited (Figure 4C and E). Next, the osteogenic related genes including β-catenin, Runx2, OCN, OPN, BMP2, osteomodulin (Figure 4F) and osteogenic related proteins including β-catenin, Runx2, BMP2 (Figure 4G and H) significantly down-regulated in BMSCs after circAars inhibition. These results suggested that circAars silencing could suppress the osteogenic differentiation capacity induced by MGO nanocomposites.

circAars Directly Sponging with miR-128-3p

CircRNAs in cytoplasm chiefly act a role as miRNAs sponges and inhibit miRNAs function.[26,27] The potential target miRNAs of circAars were predicted by TargetScan, RNAhybrid and MiRanda and seven miRNAs were found (Figure 5A). To screen the critical miRNAs that may directly bind to circAars, we applied the qPCR and discovered that miR-128-3p was significantly increasing after circAars inhibiting, whereas the other miRNAs did not obviously alter (Figure 5B). Meanwhile, the miR-128-3p and miR-3065-3p significantly decreased after being treated with MGO nanocomposites (Figure 5C). Therefore, we speculated that miR-128-3p was the only target gene of circAars in the

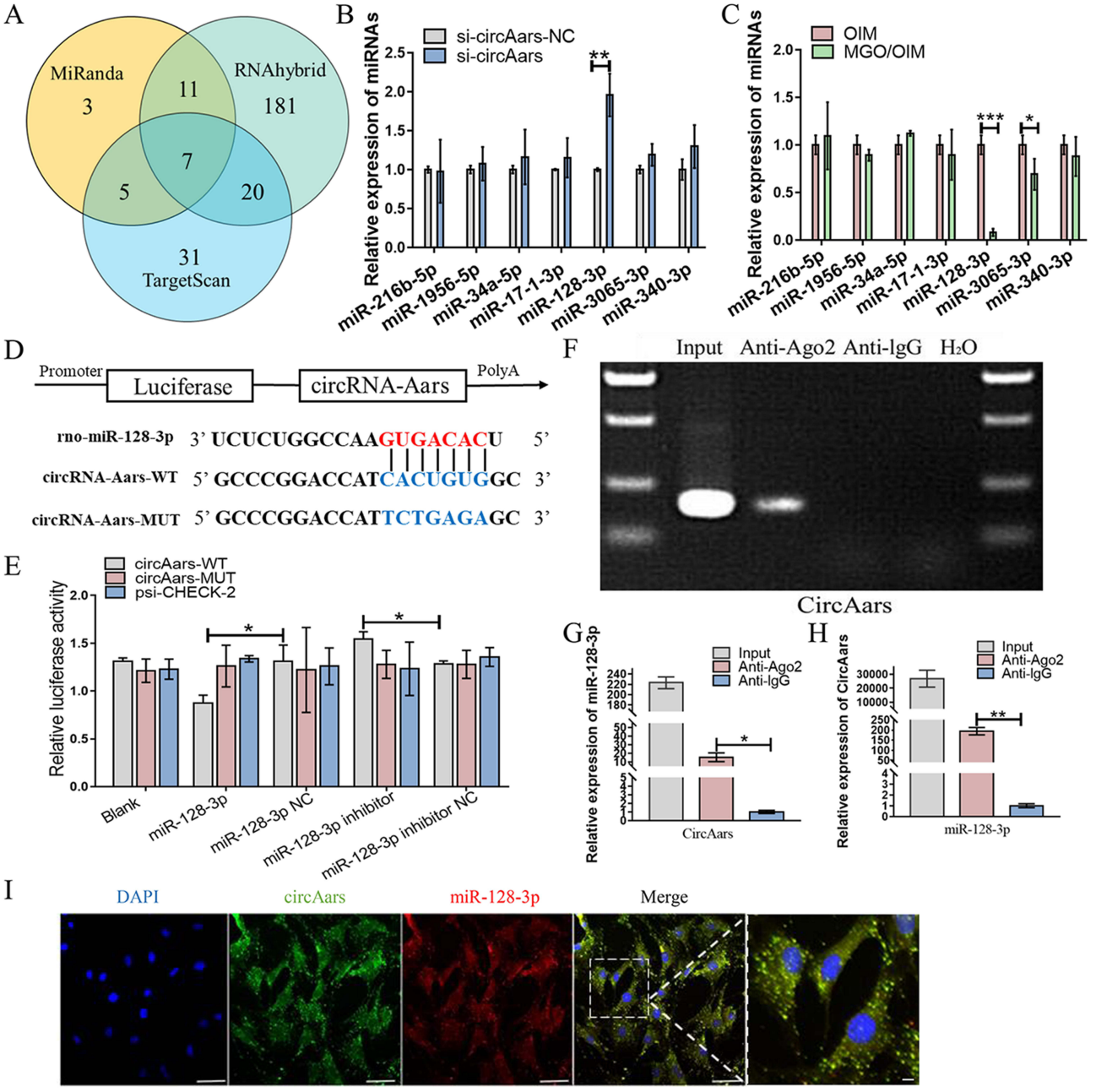

Figure 5 CircAars directly sponging with miR-128-3p. (**A**) Bioinformatics predicted potential miRNAs targets that sponged circAars. (**B**) qPCR was used to determine the expression of miRNAs in BMSCs treated with si-circAars-NC and si-circAars. (**C**) qPCR analysis of the expression of miRNAs in BMSCs cultured with OIM and MGO nanocomposites. (**D** and **E**) Schematic structure of circAars wild-type (WT) and mutant-type (MUT) luciferase reporter vectors. Luciferase activity was examined in 293T cells treated with circAars (WT/MUT) and miR-128-3p (mimic/inhibitor). (**F**–**H**) Anti-AGO2 RIP was performed in BMSCs by qPCR. (**I**) miR-128-3p co-localized with circAars in cytoplasm in BMSCs was examined through FISH. Scale bar = 50 μm. The results are presented as mean ± SD (*P<0.05, **P<0.01, ***P<0.001).

osteogenic differentiation of MGO nanocomposites. The targeted binding sequence of circAars and miR-128-3p was showed and luciferase reporter experiment revealed that the luciferase intensity of wild-type (WT) circAars sequence significantly decreased through treatment with miR-128-3p mimic and significantly increased via treatment with miR-128-3p inhibitor, but no obvious difference existed in luciferase activity of circAars mutant-type (MUT), demonstrating that miR-128-3p directly targeted the circAars (Figure 5D and E). Additionally, RIP assay was carried out in BMSCs and apparent enhancement of circAars and miR-128-3p than the controls (Figure 5F–H). Moreover, FISH demonstrated that circAars and miR-128-3p were co-existed in the cytoplasm of BMSCs (Figure 5I). These above results demonstrated that circAars could function as a sponge of miR-128-3p, which might be an important signaling pathway for MGO nanocomposites mediated osteogenic differentiation improvement effects.

circAars Inhibition Suppressed the Ability of MGO Nanocomposites Induced Osteogenic Capacity Through Sponging miR-128-3p

Considering that circAars could sponge miR-128-3p, we further explored whether circAars took its effects by sponging miR-128-3p in MGO nanocomposites induced osteogenic differentiation process. BMSCs were separately transfected with si-circAars-NC and si-circAars, co-treated with si-circAars and miR-128-3p inhibitor, and cultured in osteogenic differentiation medium with MGO. We found that ALP staining (Figure 6A) and ALP activity (Figure 6B) revealed that circAars silencing suppressed ALP activity, while the inhibiting osteogenic capacities of circAars silencing were significantly restored by miR-128-3p inhibition. Moreover, downregulation of circAars resulted in a significant mineralized nodules decreasing, but miR-128-3p inhibitor completely reversed this function (Figure 6C and D). The osteogenic genes including β-catenin, Runx2, OCN, OPN, BMP2 and osteomodulin (Figure 6E) and the proteins including β-catenin, Runx2, and BMP2 showed that miR-128-3p inhibitor partially restored the osteogenesis inhibition induced by circAars silence (Figure 6F and G). Immunofluorescence results also suggested that the expression of ALP (Figure 6H and I) and Runx2 (Figure 6J and K) obviously inhibited in circAars silencing group, which was restored by miR-128-3p inhibition. Taken together, these findings demonstrated that circAars/miR-128-3p signaling axis played an important role in regulating the osteogenic differentiation improvement induced by MGO nanocomposites.

Silencing miR-128-3p Promoted Osteogenic Capacity of MGO Nanocomposites by Increasing SMAD5

CircRNAs existing in the cytoplasm usually acts as miRNA "sponges", which can competitively bind with the target binding sites of miRNAs, thus further relieve the inhibiting downstream mRNA expression. SMAD5 is an important endogenous signal transforming growth factor in TGF-β family, which plays an important role in regulating osteogenic differentiation of stem cells.[28] miR-128-3p mimic could significantly influence the expression of SMAD2, SMAD5 and SMAD9 in non-small cell lung cancer A549 cell line.[29] To determine whether SMAD5 is a direct binding gene of miR-128-3p, the miR-128-3p inhibitor or mimic was transfected in cells containing MUT sequence and the WT sequence of SMAD5 through a luciferase reporter assay. It revealed that miR-128-3p inhibitor significantly increased the luciferase intensity and miR-128-3p mimic significantly decreased the luciferase intensity of SMAD5-WT when those were compared with the control group; however, no significant effect was found on the luciferase intensity of SMAD5-MUT (Figure 7A and B). Furthermore, we determined that the expression of SMAD5 could significantly inhibit in BMSCs by qPCR (Figure 7C) and western-blot assay (Figure 7D and E). To determine whether miR-128-3p inhibition inducing the osteogenic capacity of MGO nanocomposites was through SMAD5, BMSCs separately transfected with si-SMAD5-NC and si-SMAD5 and co-treated with si-SMAD5 and miR-128-3p inhibitor. ALP staining (Figure 7F) and ALP activity (Figure 7H) showed that SMAD5 inhibition suppressed ALP expression, while the functions of SMAD5 silencing were obviously rescued by miR-128-3p inhibitor. Moreover, down-regulation of SMAD5 resulted in a significant mineralized nodules decreasing, while miR-128-3p inhibitor partially restored this function (Figure 7G and I). Additionally, the results of the osteogenic genes expression including SMAD5, Runx2, OCN, OPN, osteomodulin (Figure 7J) and proteins expression including SMAD5, Runx2 revealed that miR-128-3p inhibitor rescued the osteogenic capacity inhibition induced by SMAD5 silencing (Figure 7K and L). Immunofluorescence staining results also

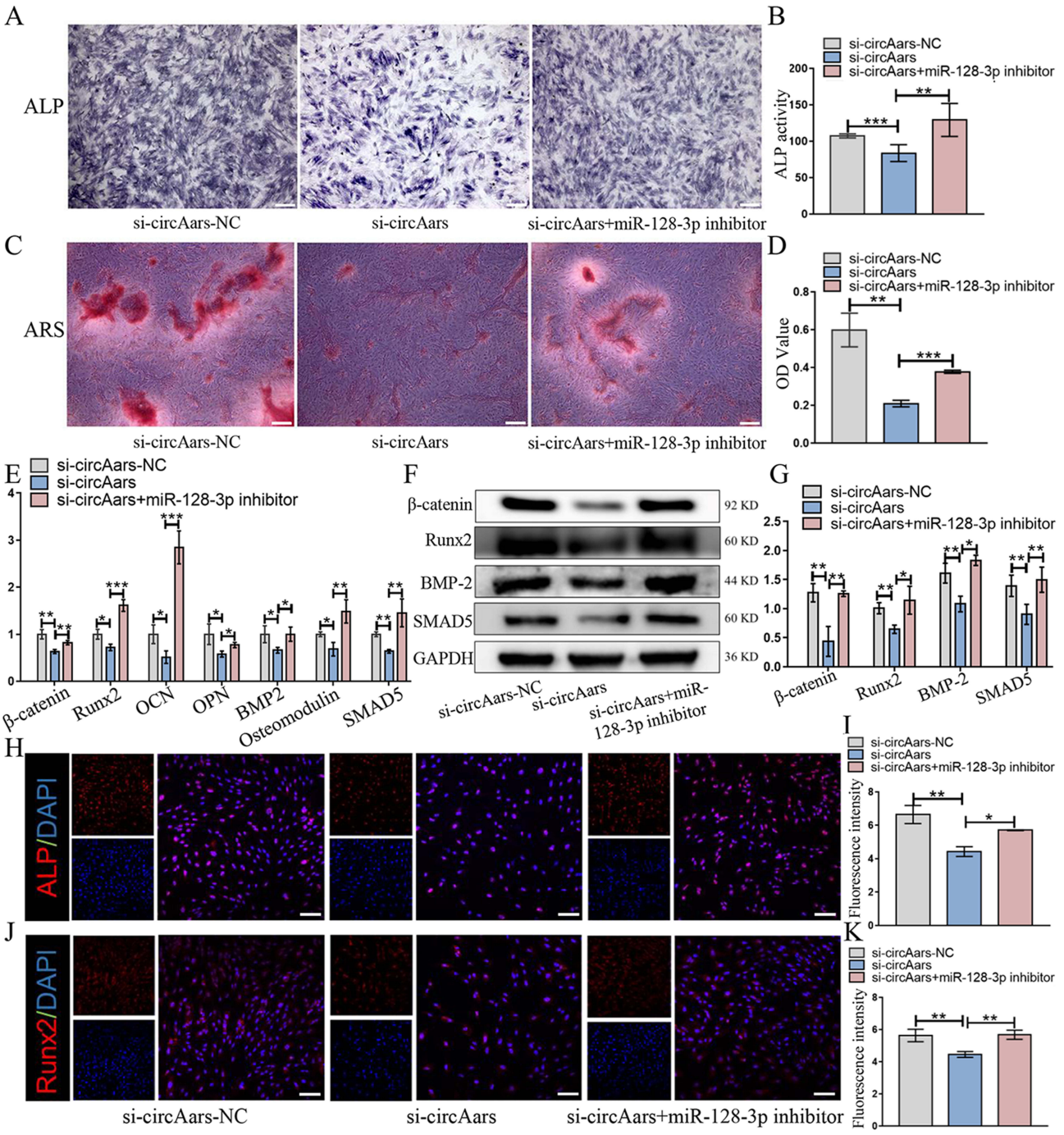

Figure 6 CircAars inhibition suppressed the ability of MGO nanocomposites induced osteogenic capacity through sponging miR-128-3p. (**A** and **B**) The ALP staining and quantitative analysis of BMSCs transfected with si-circAars-NC, si-circAars and co-treated with si-circAars and miR-128-3p inhibitor under MGO condition. Scale bar = 200 μm. (**C** and **D**) ARS staining and semi-quantitative analysis evaluated the effect of osteogenic capacity in BMSCs. Scale bar = 200 μm. (**E**) The osteogenic-related mRNA expression level was examined in BMSCs by qPCR. (**F** and **G**) The osteogenic-related proteins expression was determined by western-blot. (**H** and **I**) Immunofluorescence staining demonstrating the cellular levels of ALP and (**J** and **K**) Runx2. Scale bar = 100 μm. The results are presented as mean ± SD (*P<0.05, **P<0.01, ***P<0.001).

demonstrated the expression of SMAD5 (Figure 7M and N), ALP (Figure 7O and P) and Runx2 (Figure 7Q and R) obviously inhibited in SMAD5 silencing group, which could be partially restored by being co-treated with miR-128-3p inhibitor. Taken together, these findings suggested that SMAD5 silencing suppressed the ability of MGO nanocomposites to induce osteogenic capacity, which could be partially restored by downregulating miR-128-3p.

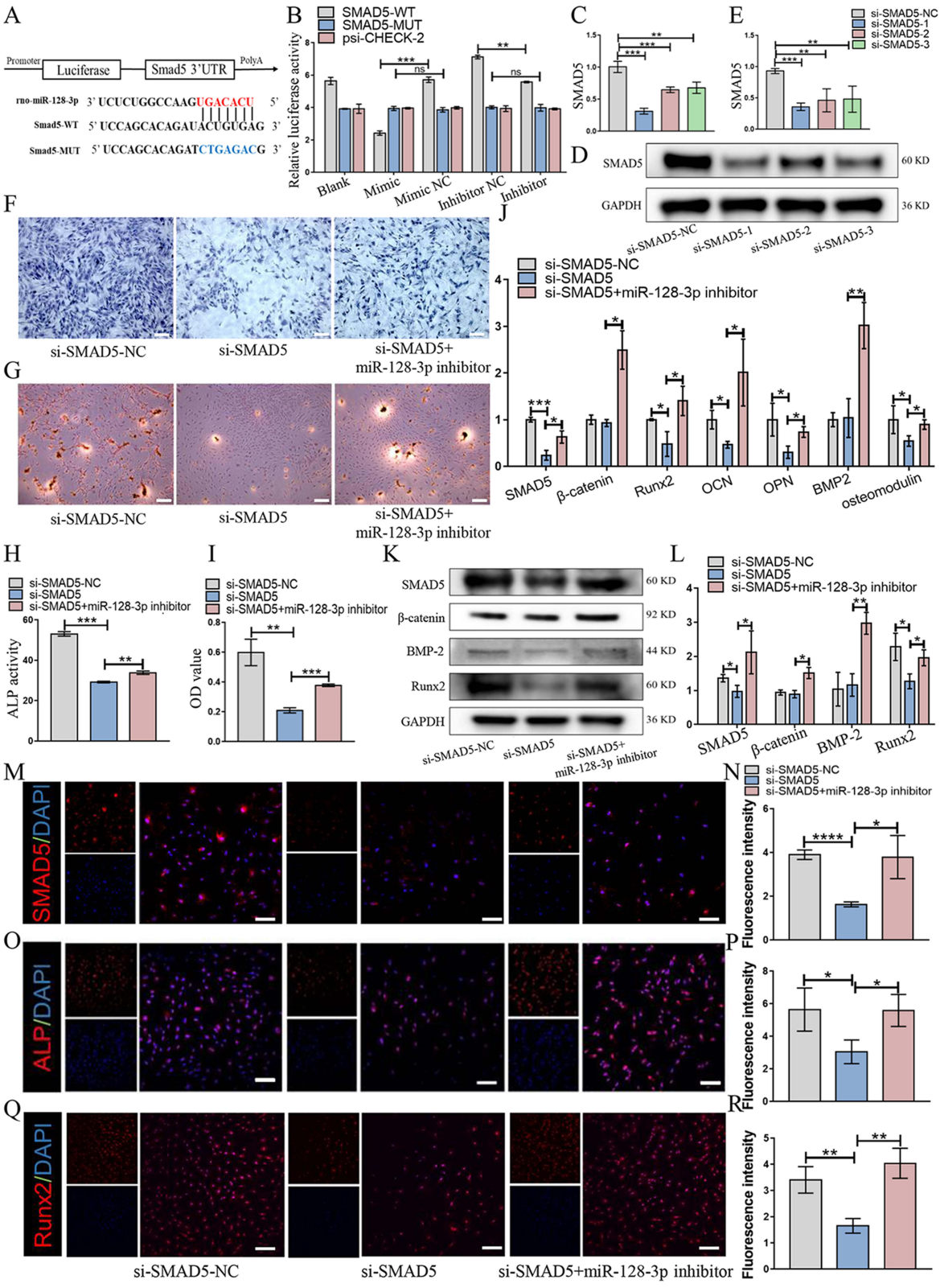

Figure 7 Silencing miR-128-3p promoted osteogenic capacity of MGO nanocomposites by increasing SMAD5. (**A** and **B**) Schematic structure of SMAD5 WT and MUT luciferase reporter vectors. Luciferase activities were examined in 293T cells treated with SMAD5 (WT/MUT) and miR-128-3p (mimic/inhibitor). (**C**) The knock-down efficiency of SMAD5 in BMSCs was identified by qPCR and (**D** and **E**) Western blot. (**F** and **H**) The ALP staining and ALP activity examination. Scale bar = 200 μm. (**G** and **I**) ARS staining and semi-quantitative analysis evaluated the effect of MGO mediated osteogenic capacity in BMSCs treated with si-SMAD5-NC, si-SMAD5 and si-SMAD5+miR-128-3p inhibitor. Scale bar = 200 μm. (**J**) The osteogenic-related mRNAs and (**K** and **L**) proteins expression level was examined in BMSCs. (**M** and **N**) Cellular immunofluorescence staining revealing the levels of SMAD5; (**O** and **P**) ALP and (**Q** and **R**) Runx2. Scale bar = 100 μm. The results are presented as mean ± SD (*P<0.05, **P<0.01, ***P<0.001, ****p < 0.0001).

circAars Upregulating SMAD5 Was Vital for Osteogenic Capacity Induced by MGO Nanocomposites

These above outcomes suggested that, in the mechanism exploration of MGO nanocomposites inducing osteogenesis in BMSCs, the circAars inhibition decreased the osteogenic capacities through upregulating miR-128-3p and meanwhile miR-128-3p inhibitor promoted the osteogenic capacity through increasing SMAD5 (Figure 8A). Therefore, we further determined the functional interrelation between the circAars and SMAD5 in MGO-mediated osteogenic differentiation. The expression of circAars was significantly upregulated determined by qPCR after transfection of circAars over-expression plasmids (Figure 8B). Upregulation of circAars significantly increased ALP activity compared with circAars-NC, whereas these effects could be significantly suppressed by SMAD5 inhibition (Figure 8C and D). Meanwhile, mineralized nodules number was more apparent in the circAars overexpression group, while SMAD5 silencing could partially suppress this effect (Figure 8E and F). The osteogenic genes including SMAD5, Runx2, OCN, OPN, osteomodulin (Figure 8G) and proteins including SMAD5, Runx2 significantly increased when overexpressing circAars, while SMAD5 silence partially suppressed these effects (Figure 8H and I). Additionally, the expression of SMAD5 (Figure 8J and K), ALP (Figure 8L and M) and Runx2 (Figure 8N and O) upregulated in immunofluorescence assay by overexpressing circAars; however, this effect partially inhibited by SMAD5 silencing. Summarization of these results determined that SMAD5 regulation by circAars was essential for the osteogenic capacity induced by MGO nanocomposites.

Craniomaxillofacial Bone Defects Repair Evaluation in vivo

Rat cranial bone defect was applied to further verify the bone repair ability of MGO nanocomposites in vivo. The results of micro-CT three-dimensional reconstruction demonstrated a greater number of new bone formation in the MGO group (Figure 9A). As showed in Figure 9B–D, the highest percentages of bone volume fraction (BV/TV), bone mineral density (BMD) and trabecular number (Tb. N) were found in MGO group. As shown in Figure 9E, abundant new bone tissue formation was found in MGO group, while only a small amount of new bone was examined in GM or OIM group after 8 weeks of treatment. As shown in Figure 9F, the number of new collagen fibers in the GM or OIM group was less than in the MGO group after 8 weeks of treatment. FISH results demonstrated that compared with GM and OIM treatment groups, MGO induced BMSCs group showed significantly improved circAars expression and inhibited miR-128-3p expression (Figure 9G and H) in the new bone repair region. Further evaluation of the bone-forming related proteins (Runx2 and SMAD5) in the new bone regeneration region with IHC staining identified more positively stained areas of Runx2 (Figure 9I and J) and SMAD5 (Figure 9K and L) in MGO groups. The above results suggested that MGO nanocomposites could improve craniomaxillofacial bone defects repair through regulating circAars/miR-128-3p/SMAD5 signaling pathway.

Discussion

MGO nanocomposites showed excellent physical and chemical characteristics, which have great potential in the biomedical field of bio-imaging, targeted drug delivery and therapy, biosensors, chemical substance extraction and separation, cancer therapy and stem cell regulation.[7,30] Compared to other bone repair materials, MGO nanoparticles have a larger specific surface area, smaller nanoparticle size, are easy to enter cells, and have ferromagnetism. They can regulate the biological functions of stem cells by combining with static magnetic field and can serve as a carrier for gene and drug transfection into cells, which has great potential for application in the field of bone tissue engineering.[31–34] However, as a kind of nanoparticles, MGO is not easily aggregated in the area of bone defects, so other scaffold materials or static magnetic fields need to be combined to repair large-scale bone defects.[7,35,36] Therefore, whether MGO has potential in BTE for craniomaxillofacial bone repair is worth further exploration. Because of the multidirectional differentiation potential, BMSCs are considered as candidates in bone regeneration. In this study, low concentration of MGO nanocomposites was unable to affect the viability, adherent numbers and proliferative potential of BMSCs. However, it indeed promoted osteogenic capacity of BMSCs according to ALP and ARS staining results observed, which was most significant in 0.1 μg/mL MGO group (Figure 2). These might be attributed to the stronger potential of

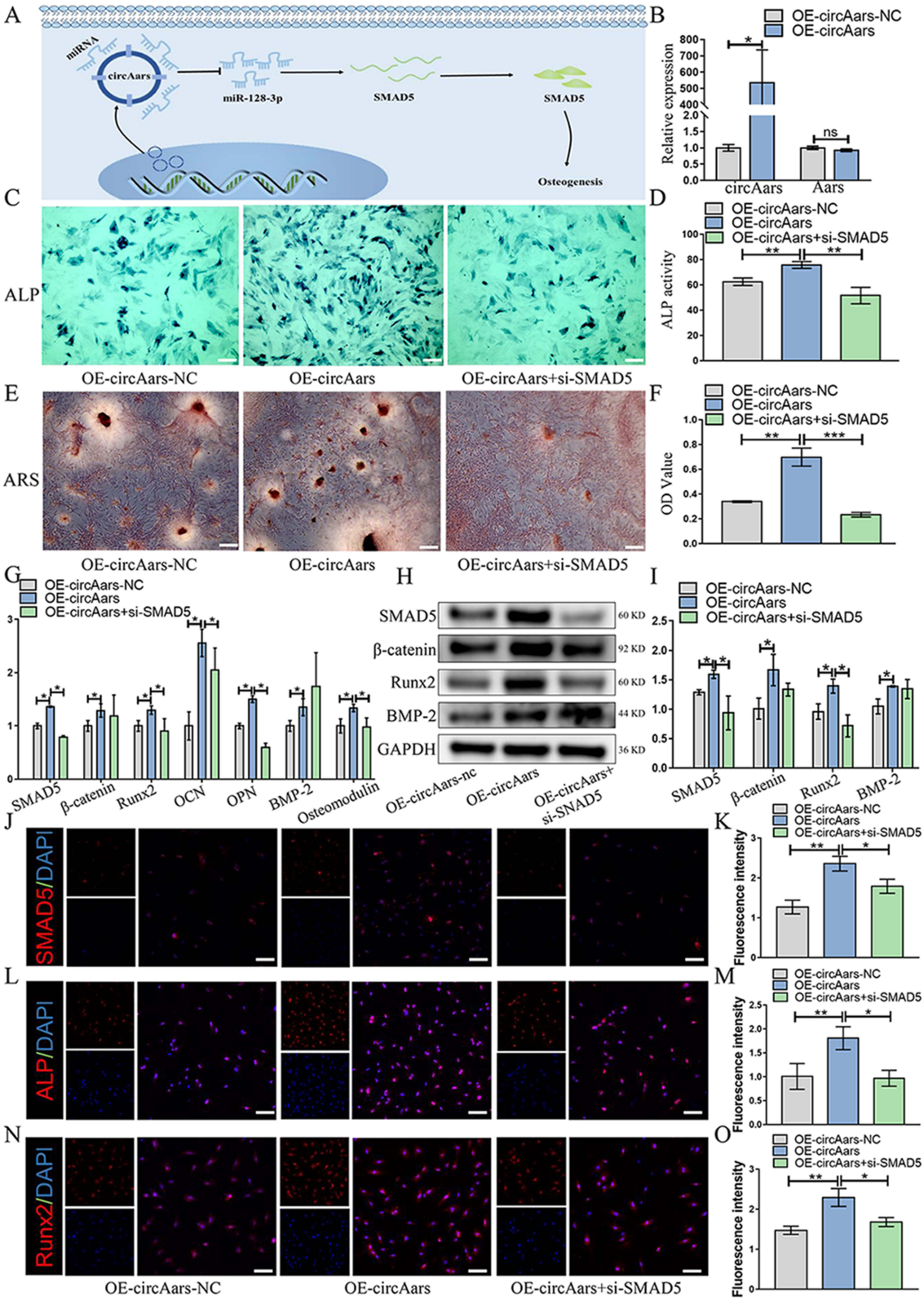

Figure 8 CircAars upregulating SMAD5 was vital for osteogenic capacity induced by MGO nanocomposites. (**A**) Schematic illustration of the circAars sponging miR-128-3p to regulate the expression of SMAD5, which participate in osteogenic process in BMSCs. (**B**) The overexpression efficiency of circAars in BMSCs examined. (**C** and **D**) The ALP staining and quantitative analysis of BMSCs treated with OE-circAars-NC, OE-circAars and OE-circAars+si-SMAD5. Scale bar = 200 μm. (**E** and **F**) ARS staining and semi-quantitative analysis evaluated the effect of osteogenic capacity in BMSCs. Scale bar = 200 μm. (**G**) The osteogenic-related mRNAs and (**H** and **I**) proteins expression was examined in BMSCs. (**J** and **K**) Immunofluorescence results demonstrating the cellular expression levels of SMAD5; (**L** and **M**) ALP and (**N** and **O**) Runx2. The results are presented as mean ± SD (*P<0.05, **P<0.01, ***P<0.001).

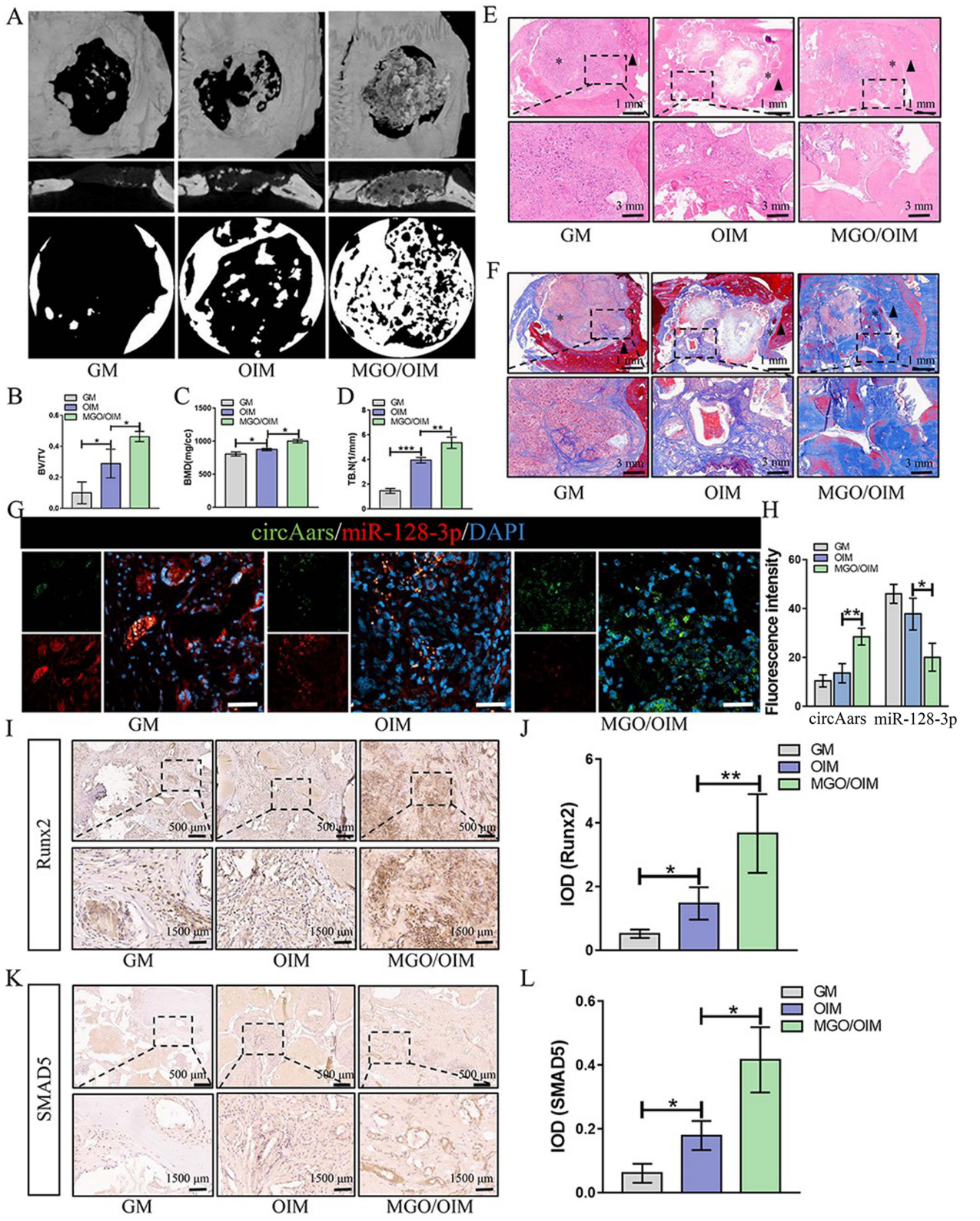

Figure 9 Craniomaxillofacial bone defects repair evaluation in vivo. (**A**) Micro-CT revealed that new bone formation ability. (**B**–**D**) Micro-CT quantitative results demonstrated the BV/TV, BMD, TB.N. (**E**) H&E staining and (**D**) Masson's trichrome staining for new bone regeneration. Star: new bone; triangle: native bone. Scale bar = 1 mm. (**G** and **H**) Representative FISH staining images of circAars and miR-128-3p in the defect position. Scale bar = 50 μm. (**I** and **J**) Representative immune-histochemical images of Runx2 and (**K** and **L**) SMAD5 in the defect position. The results are presented as mean ± SD (*P<0.05, **P<0.01).

0.1 μg/mL MGO to induce BMSCs proliferation. The expression and activity of ALP were obviously accelerated in the early stage of calcification, which is an early marker of mineralization.[37] ARS staining examined matrix mineralization degree, which is a marker of late osteogenic differentiation.[38] In this study, osteogenesis markers (eg, β-catenin, Runx2, BMP2, OPN, OCN and osteomodulin) were found to be positively regulated by MGO nanocomposites, further confirming our findings. The above in vitro experiments showed that MGO nanocomposites had good biocompatibility and could induce osteogenic differentiation of BMSCs which is consistent with what reported earlier.[8,39] In addition, the critical-sized craniomaxillofacial bone defects in rats by cell scaffold material were established. Micro-CT and histological examination results were consistent with the in vitro conclusions (Figure 9). Taken together, these findings indicated that MGO nanocomposites have the ability to improve the stem cells osteogenic differentiation, further promote repair of craniomaxillofacial bone defects.

CircRNAs are special kind of noncoding RNA molecule, which is expressed specifically in cells or tissues and performs various regulatory functions. Unlike linear RNA, circRNAs have an intact circular structure and can avoid degradation by exonucleases.[40] CircRNAs are extremely stable in living cells and with well-defined functions can be used not only as biomarkers for the diagnosis but also as therapeutic targets for some important diseases, especially immune diseases and cancers.[41,42] Recently, increasing studies showed that circRNAs hold potential, important and functional effect on managing cellular behaviors and osteogenic differentiation.[43] Whether circRNAs play an essential role in the regulation of osteogenesis in MGO nanocomposites induced BMSCs is worth exploring. Using high-throughput RNA sequencing technique, a new circRNA, termed "circAars", was found and identified, which showed a ring structure and resisted to RNase and mainly existed in cytoplasm (Figure 3). CircAars silencing decreased the osteogenic differentiation capacity of BMSCs under osteogenic medium, which suggested that circAars might play an important role in the osteogenesis. In addition, we found that circAars inhibition suppressed the osteogenic capacity of BMSCs induced by MGO nanocomposites (Figure 4). These results further suggested that circRNAs, especially circAars played an important role in regulating stem cells osteogenic differentiation by MGO nanocomposites, which is similar with the studies reported.[44,45] Chen et al also showed that a total of 17 circRNAs were found with significant differences in glucocorticoid-induced osteoporosis rat groups compared with normal groups through RNA sequencing. Meanwhile, circARSB could suppress, and circPTEN could promote BMSCs osteogenic differentiation.[44] Zhang et al found that overexpressing circ-CTTN could promote osteogenic effect in vitro. In the rat calvarial defect model, the overexpressing circ-CTTN group presented a larger bone healing volume and denser bone trabecular distribution than other groups.[45] The above studies indicate that circRNA can regulate the osteogenic differentiation of stem cells and thus have great application prospects in bone tissue engineering.

How does circAars participate in MGO-induced osteogenic differentiation? In recent years, increasing evidences have suggested that circRNAs existing in the cytoplasm usually act as miRNA 'sponges', which can competitively bind with the target binding sites of miRNAs, thus further managing the expression level of the mRNAs.[46,47] For examples, circ-0074834 promoted osteogenic capacity of BMSCs and the treatment of bone defects, which acted as a ceRNA to modulate the level of VEGF and ZEB1 by miR-942-5p.[48] Chen et al found that circRNA CDR1as improved adipogenic differentiation and suppressed osteogenesis of BMSCs in steroid-induced osteonecrosis of the femoral head via miR-7-5p/WNT5B pathway.[49] These findings suggested that circRNAs could play a crucial effect in the field of bone regeneration through ceRNA interaction mechanism. In this study, for screening the underlying miRNA of circAars, applying TargetScan, miRanda and RNAhybrid, we found a putative circAars-miRNAs connection network at the basis of the complementary matching sequence. Subsequently, we determined that circAars acted as an endogenous sponge for miR-128-3p through qPCR, the luciferase reporter experiment, RIP examination, and FISH detection (Figure 5).

Emerging evidences suggested miRNAs serve a crucial part in regulating cellular behavior and multidirectional differentiation of stem cells.[50–52] Interestingly, Xu et al suggested that miR-128-3p apparently increased in aged-exosomes by using miRNA array analysis, and further found that SMAD5 was a direct target gene of miR-128-3p, which could be suppressed by overexpressing miR-128-3p.[53] However, whether miR-128-3p could manage MGO nanocomposites osteogenic behaviors has been never investigated. In our study, we verified that down-regulation of miR-128-3p could rescue the function of circAars inhibition, further demonstrating that circAars might enhance osteogenic differentiation through sponging miR-128-3p in MGO nanocomposites mediated BMSCs (Figure 6). Taken

together, these findings demonstrated that circAars/miR-128-3p signaling axis played an important role in regulating the osteogenic improvement induced by MGO nanocomposites.

Moreover, for exploring indepth the regulatory underlying mechanisms between circAars and miR-128-3p, we demonstrated that miR-128-3p had definitive connecting position with SMAD5 and negatively managed its level through the luciferase reporter experiment, qPCR, and western-blot assay, which is conformed with the results reported earlier.[53] As we known, SMAD5 pertains to the receptor-activated SMAD that serving as intracellular signal transducers for TGF-β superfamily, which are the immediate downstream molecules of BMP receptors and act a critical role in BMP signal transduction.[28,54] Gu et al found that TGF-β family was regulated by miR-128-3p. miR-128-3p mimic could significantly reduce the expression of SMAD2, SMAD5 and SMAD9 in non-small cell lung cancer A549 cell line. However, miR-128-3p inhibitor significantly promoted the expression of SMAD2, SMAD5 and SMAD9.[29] However, whether miR-128-3p could regulate MGO nanocomposites mediated BMSCs osteogenic behaviors via regulating SMAD5 has not been fully clarified. Interestingly, we found that circAars overexpression could positively improve SMAD5 activity and the miR-128-3p negatively manage the level of SMAD5. Functionally, SMAD5 silencing in BMSCs suppressed osteogenic differentiation induced by MGO nanocomposites, which could be partially restored through miR-128-3p suppression (Figure 7). Meanwhile, SMAD5 silence in BMSCs could abolish the effects of circAars overexpression in osteogenic differentiation promotion induced by MGO nanocomposites (Figure 8). In addition, in vivo experiments showed that the expressions of circAars and SMAD5 were significantly enhanced in the new region of craniomaxillofacial bone tissue in the MGO group, while the expression of miR-128-3p was significantly weakened, which were consistent with the in vitro results (Figure 9). The above results suggested that MGO nanocomposites could improve craniomaxillofacial bone defects repair through regulating circAars/miR-128-3p/SMAD5 signaling pathway.

Conclusion

In summary, our results suggested that MGO nanocomposites were good biocompatible with BMSCs and could promote the osteogenic ability of BMSCs to repair craniomaxillofacial bone defects. More important, a new circRNA-circAars was found and further identified. Mechanistically, circAars could sponge miR-128-3p in turn to regulate the expression of SMAD5, which played a critical role in MGO-induced craniomaxillofacial bone regeneration process. This study could not only provide a feasible and effective strategy to repair the critical-sized craniomaxillofacial bone defects but also offer a theoretical basis for the development of bone regeneration nanomaterials based on regulation of circAars.

Data Sharing Statement

The RNA sequencing data was uploaded in Sequence Read Archive database of NCBI (https://www.ncbi.nlm.nih.gov/sra/PRJNA886454). The other datasets used during the current study are available from the corresponding authors on reasonable request.

Acknowledgments

This work was supported by grants from the National Natural Science Foundation of China (82073378; 82373255); The Guangdong Basic and Applied Basic Research Foundation Project (2021A1515012399; 2021A1515110267).

Disclosure

The authors declare that they have no known competing financial interests or personal relationships that could have appeared to influence the work reported in this paper.

References

1. ElHawary H, Baradaran A, Abi-Rafeh J, Vorstenbosch J, Xu L, Efanov JI. Bone healing and inflammation: principles of fracture and repair. *Sem Plast Surg*. 2021;35(3):198–203. doi:10.1055/s-0041-1732334
2. Chen Y, Xu J, Huang Z, et al. An innovative approach for enhancing bone defect healing using PLGA Scaffolds Seeded with extracorporeal-shock-wave-treated Bone Marrow Mesenchymal Stem Cells (BMSCs). *Sci Rep*. 2017;7(1):44130. doi:10.1038/srep44130
3. Roseti L, Parisi V, Petretta M, et al. Scaffolds for bone tissue engineering: state of the art and new perspectives. *Mater Sci Eng C Mater Biol Appl*. 2017;78:1246–1262. doi:10.1016/j.msec.2017.05.017

4. Eini E, Ghaemi A, Rahim F. Bone using stem cells for maxillofacial bone disorders: a systematic review and meta-analysis. In: *Advances in Experimental Medicine and Biology*. Springer; 2022.
5. Ma R, Su Y, Cao R, Wang K, Yang P. Enhanced osteogenic activity and bone repair ability of PLGA/MBG scaffolds doped with ZIF-8 nanoparticles loaded with BMP-2. *Int J Nanomed*. 2023;18:5055–5072. doi:10.2147/IJN.S423985
6. Dong Y, Yao L, Cai L, et al. Antimicrobial and pro-osteogenic coaxially electrospun magnesium oxide nanoparticles-polycaprolactone/parathyroid hormone-polycaprolactone composite barrier membrane for guided bone regeneration. *Int J Nanomed*. 2023;18:369–383. doi:10.2147/IJN.S395026
7. He Y, Yi C, Zhang XL, Zhao W, Yu DS. Magnetic graphene oxide: synthesis approaches, physicochemical characteristics, and biomedical applications. *Trac-Trends Anal Chem*. 2021;136:116191. doi:10.1016/j.trac.2021.116191
8. Zhang W, Yang G, Wang X, et al. Magnetically controlled growth-factor-immobilized multilayer cell sheets for complex tissue regeneration. *Adv Mater*. 2017;29(43). doi:10.1002/adma.201703795
9. Zhang H, Li S, Liu Y, et al. Fe(3)O(4)@GO magnetic nanocomposites protect mesenchymal stem cells and promote osteogenic differentiation of rat bone marrow mesenchymal stem cells. *Biomater Sci*. 2020;8(21):5984–5993. doi:10.1039/D0BM00906G
10. He Y, Chen G, Li Y, et al. Effect of magnetic graphene oxide on cellular behaviors and osteogenesis under a moderate static magnetic field, Nanomedicine. *Nanotechnol Biol Med*. 2021;37:102435. doi:10.1016/j.nano.2021.102435
11. Hombach S, Kretz M. Non-coding RNAs: classification, biology and functioning. *Adv Exp Med Biol*. 2016;937:3–17.
12. Yuan YG, Zhang YX, Liu SZ, et al. Multiple RNA profiling reveal epigenetic toxicity effects of oxidative stress by graphene oxide silver nanoparticles in-vitro. *Int J Nanomed*. 2023;18:2855–2871. doi:10.2147/IJN.S373161
13. Chen X, Peng Y, Xue H, Liu G, Wang N, Shao Z. MiR-21 regulating PVT1/PTEN/IL-17 axis towards the treatment of infectious diabetic wound healing by modified GO-derived biomaterial in mouse models. *J Nanobiotechnol*. 2022;20(1):309. doi:10.1186/s12951-022-01516-4
14. Kristensen LS, Andersen MS, Stagsted LVW, Ebbesen KK, Hansen TB, Kjems J. The biogenesis, biology and characterization of circular RNAs, Nature reviews. *Genetics*. 2019;20(11):675–691. doi:10.1038/s41576-019-0158-7
15. Guo Z, Zhao L, Ji S, et al. CircRNA-23525 regulates osteogenic differentiation of adipose-derived mesenchymal stem cells via miR-30a-3p. *Cell Tissue Res*. 2021;383(2):795–807. doi:10.1007/s00441-020-03305-7
16. Yang J, Cheng M, Gu B, Wang J, Yan S, Xu D. CircRNA_09505 aggravates inflammation and joint damage in collagen-induced arthritis mice via miR-6089/AKT1/NF-κB axis. *Cell Death Dis*. 2020;11(10):833. doi:10.1038/s41419-020-03038-z
17. Huang HB, Luo HT, Wei NN, et al. Integrative analysis reveals a lineage-specific circular RNA landscape for adipo-osteogenesis of human mesenchymal stem cells. *Stem Cell Res Ther*. 2022;13(1):106. doi:10.1186/s13287-022-02792-5
18. Zhao X, Sun W, Guo B, Cui L. Circular RNA BIRC6 depletion promotes osteogenic differentiation of periodontal ligament stem cells via the miR-543/PTEN/PI3K/AKT/mTOR signaling pathway in the inflammatory microenvironment. *Stem Cell Res Ther*. 2022;13(1):417. doi:10.1186/s13287-022-03093-7
19. Wang T, Li C, Shi M, Zhou S, Chen J, Wang F. Circular RNA circZNF532 facilitates angiogenesis and inflammation in diabetic retinopathy via regulating miR-1243/CARM1 axis. *Diabetol Metab Syndr*. 2022;14(1):14. doi:10.1186/s13098-022-00787-z
20. Wang Y, Jiang Z, Yu M, Yang G. Roles of circular RNAs in regulating the self-renewal and differentiation of adult stem cells. *Differentiation*. 2020;113:10–18. doi:10.1016/j.diff.2020.03.001
21. Kristensen LS, Okholm TLH, Veno MT, Kjems J. Circular RNAs are abundantly expressed and upregulated during human epidermal stem cell differentiation. *RNA Biol*. 2018;15(2):280–291. doi:10.1080/15476286.2017.1409931
22. Liu CX, Li X, Nan F, et al. Structure and degradation of circular RNAs regulate PKR activation in innate immunity. *Cell*. 2019;177(4):865–880. e21. doi:10.1016/j.cell.2019.03.046
23. Chen X, Yang T, Wang W, et al. Circular RNAs in immune responses and immune diseases. *Theranostics*. 2019;9(2):588–607. doi:10.7150/thno.29678
24. Min X, Liu DL, Xiong XD. Circular RNAs as competing endogenous RNAs in cardiovascular and cerebrovascular diseases: molecular mechanisms and clinical implications. *Front Cardiovasc Med*. 2021;8:682357. doi:10.3389/fcvm.2021.682357
25. Zhang D, Ni N, Wang Y, et al. CircRNA-vgll3 promotes osteogenic differentiation of adipose-derived mesenchymal stem cells via modulating miRNA-dependent integrin α5 expression. *Cell Death Differ*. 2020;28(1):283–302. doi:10.1038/s41418-020-0600-6
26. Panda AC. Circular RNAs act as miRNA sponges. *Adv Exper Med Biol*. 2018;1087:67–79.
27. Ping J, Li L, Dong Y, et al. The role of long non-coding RNAs and circular RNAs in bone regeneration: modulating miRNAs function. *J Tissue Eng Regener Med*. 2021;16(3):227–243. doi:10.1002/term.3277
28. Liu B, Mao N. Smad5: signaling roles in hematopoiesis and osteogenesis. *Int J Biochem Cell Biol*. 2004;36(5):766–770. doi:10.1016/S1357-2725(03)00250-4
29. Gu M, Wang X, Ding X. Pseudogene MSTO2P Interacts with miR-128-3p to regulate coptisine sensitivity of Non-Small-Cell Lung Cancer (NSCLC) through TGF-β signaling and VEGFC. *J Oncol*. 2022;2022:9864411. doi:10.1155/2022/9864411
30. Qian G, Zhang L, Li X, Shuai C, Wang X. Construction of Fe(3)O(4)-loaded mesoporous carbon systems for controlled drug delivery. *ACS Appl Bio Mater*. 2021;4(6):5304–5311. doi:10.1021/acsabm.1c00422
31. Qian G, Mao Y, Zhao H, Zhang L, Xiong L, Long Z. pH-Responsive nanoplatform synergistic gas/photothermal therapy to eliminate biofilms in poly(L-lactic acid) scaffolds. *J Mater Chem B*. 2024;12(5):1379–1392. doi:10.1039/D3TB02600K
32. Qian G, Mao Y, Shuai Y, Zeng Z, Peng S, Shuai C. Enhancing bone scaffold interfacial reinforcement through in situ growth of metal-organic frameworks (MOFs) on strontium carbonate: achieving high strength and osteoimmunomodulation. *J Colloid Interface Sci*. 2024;655:43–57. doi:10.1016/j.jcis.2023.10.133
33. He Y, Shi F, Hu J, et al. Magnetic graphene oxide nanocomposites induce cytotoxicity in ADSCs via GPX4 regulating ferroptosis. *Ecotoxicol Environ Saf*. 2023;269:115745. doi:10.1016/j.ecoenv.2023.115745
34. Liu CH, Chen YJ, Wu WC, Lin YH. Magnetic graphene oxide nanoflakes for dual RNA interfering delivery and gene knockdown in prostate and liver cancers. *Int J Biol Macromol*. 2023;253(Pt 8):127357. doi:10.1016/j.ijbiomac.2023.127357
35. Ma J, Zhang M, Ji M, et al. Magnetic graphene oxide-containing chitosan-sodium alginate hydrogel beads for highly efficient and sustainable removal of cationic dyes. *Int J Biol Macromol*. 2021;193(Pt B):2221–2231. doi:10.1016/j.ijbiomac.2021.11.054
36. Zhou P, Yan B, Wei B, et al. Quercetin-solid lipid nanoparticle-embedded hyaluronic acid functionalized hydrogel for immunomodulation to promote bone reconstruction. *Regen Biomater*. 2023;10:rbad025. doi:10.1093/rb/rbad025

37. Halling Linder C, Ek-Rylander B, Krumpel M, et al. Bone alkaline phosphatase and tartrate-resistant acid phosphatase: potential co-regulators of bone mineralization. *Calcif Tissue Int*. 2017;101(1):92–101. doi:10.1007/s00223-017-0259-2
38. Guan H, Kong N, Tian R, et al. Melatonin increases bone mass in normal, perimenopausal, and postmenopausal osteoporotic rats via the promotion of osteogenesis. *J Transl Med*. 2022;20(1):132. doi:10.1186/s12967-022-03341-7
39. He Y, Li Y, Chen G, et al. Concentration-dependent cellular behavior and osteogenic differentiation effect induced in bone marrow mesenchymal stem cells treated with magnetic graphene oxide. *J Biomed Mater Res Part A*. 2019;108(1):50–60. doi:10.1002/jbm.a.36791
40. Misir S, Wu N, Yang BB. Specific expression and functions of circular RNAs. *Cell Death Differ*. 2022;29(3):481–491. doi:10.1038/s41418-022-00948-7
41. Zhang S, Sun J, Gu M, Wang G, Wang X. Circular RNA: a promising new star for the diagnosis and treatment of colorectal cancer. *Cancer Med*. 2021;10(24):8725–8740. doi:10.1002/cam4.4398
42. Rong Z, Xu J, Shi S, et al. Circular RNA in pancreatic cancer: a novel avenue for the roles of diagnosis and treatment. *Theranostics*. 2021;11(6):2755–2769. doi:10.7150/thno.56174
43. Huang W, Wu Y, Qiao M, et al. CircRNA-miRNA networks in regulating bone disease. *J Cell Physiol*. 2021;237(2):1225–1244. doi:10.1002/jcp.30625
44. Chen Z, Lin W, Zhao S, et al. Identification of circRNA expression profiles in BMSCs from glucocorticoid-induced osteoporosis model. *Stem Cells Int*. 2022;2022:3249737. doi:10.1155/2022/3249737
45. Zhang M, He Y, Zhang X, et al. Engineered cell-overexpression of circular RNA hybrid hydrogels promotes healing of calvarial defects. *Biomater Sci*. 2023;11(5):1665–1676. doi:10.1039/D2BM01472F
46. Mohanapriya R, Akshaya RL, Selvamurugan N. A regulatory role of circRNA-miRNA-mRNA network in osteoblast differentiation. *Biochimie*. 2021;193:137–147. doi:10.1016/j.biochi.2021.11.001
47. Chen G, Li Y, He Y, et al. Upregulation of circular RNA circATRNL1 to sensitize oral squamous cell carcinoma to irradiation. *Mol Ther Nucleic Acids*. 2020;19:961–973. doi:10.1016/j.omtn.2019.12.031
48. Ouyang Z, Tan T, Zhang X, et al. CircRNA hsa_circ_0074834 promotes the osteogenesis-angiogenesis coupling process in bone mesenchymal stem cells (BMSCs) by acting as a ceRNA for miR-942-5p. *Cell Death Dis*. 2019;10(12):932. doi:10.1038/s41419-019-2161-5
49. Chen G, Wang Q, Li Z, et al. Circular RNA CDR1as promotes adipogenic and suppresses osteogenic differentiation of BMSCs in steroid-induced osteonecrosis of the femoral head. *Bone*. 2020;133:115258. doi:10.1016/j.bone.2020.115258
50. Moghaddam T, Neshati Z. Role of microRNAs in osteogenesis of stem cells. *J Cell Biochem*. 2019;120(8):14136–14155. doi:10.1002/jcb.28689
51. Lv Y, Huang Y, Xu M, et al. The miR-193a-3p-MAP3k3 signaling axis regulates substrate topography-induced osteogenesis of bone marrow stem cells. *Adv Sci*. 2020;7(1):1901412. doi:10.1002/advs.201901412
52. Yan J, Lu X, Zhu X, et al. Effects of miR-26a on osteogenic differentiation of bone marrow mesenchymal stem cells by a mesoporous silica nanoparticle - PEI - Peptide System. *Int J Nanomed*. 2020;15:497–511. doi:10.2147/IJN.S228797
53. Xu T, Luo Y, Wang J, et al. Exosomal miRNA-128-3p from mesenchymal stem cells of aged rats regulates osteogenesis and bone fracture healing by targeting Smad5. *J Nanobiotechnol*. 2020;18(1):47. doi:10.1186/s12951-020-00601-w
54. Chen D, Zhao M, Mundy GR. Bone morphogenetic proteins. *Growth Factors*. 2004;22(4):233–241. doi:10.1080/08977190412331279890